Non-protein amino acids identified in carbon-rich Hayabusa particles

Eric T. PARKER [iD]*[1], Queenie H. S. CHAN [iD][2,3], Daniel P. GLAVIN [iD][1], and
Jason P. DWORKIN [iD][1]

[1]Astrobiology Analytical Laboratory, Solar System Exploration Division, NASA Goddard Space Flight Center, Greenbelt,
Maryland 20771, USA
[2]Department of Earth Sciences, Royal Holloway University of London, Egham, Surrey TW20 0EX, UK
[3]School of Physical Sciences, The Open University, Walton Hall, Milton Keynes MK7 6AA, UK
*Corresponding author. E-mail: eric.t.parker@nasa.gov

Abstract–Amino acid abundances in acid-hydrolyzed hot water extracts of gold foils containing five Category 3 (carbon-rich) Hayabusa particles were studied using liquid chromatography with tandem fluorescence and accurate mass detection. Initial particle analyses using field emission scanning electron microscopy with energy-dispersive X-ray spectrometry indicated that the particles were composed mainly of carbon. Prior to amino acid analysis, infrared and Raman microspectroscopy showed some grains possessed primitive organic carbon. Although trace terrestrial contamination, namely L-protein amino acids, was observed in all Hayabusa extracts, several terrestrially uncommon non-protein amino acids were also identified. Some Hayabusa particles contained racemic (D≈L) mixtures of the non-protein amino acids β-aminoisobutyric acid (β-AIB) and β-amino-*n*-butyric acid (β-ABA) at low abundances ranging from 0.09 to 0.31 nmol g^{-1}. Larger abundances of the non-protein amino acid β-alanine (9.2 nmol g^{-1}, ≈4.5 times greater than background levels) were measured in an extract of three Hayabusa particles. This β-alanine abundance was ≈6 times higher than that measured in an extract of a CM2 Murchison grain processed in parallel. The comparatively high β-alanine abundance is surprising as asteroid Itokawa is similar to amino acid-poor LL ordinary chondrites. Elevated β-alanine abundances and racemic β-AIB and β-ABA in Hayabusa grains suggested these compounds have non-biological and plausibly non-terrestrial origins. These results are the first evidence of plausibly extraterrestrial amino acids in asteroid material from a sample-return mission and demonstrate the capabilities of the analytical protocols used to study asteroid Ryugu and Bennu samples returned by the JAXA Hayabusa2 and NASA OSIRIS-REx missions, respectively.

INTRODUCTION

Small primitive bodies, including asteroids and comets, are composed of chemical constituents from the early solar system and offer a glimpse at the prebiotic chemical inventory of the planets at or near the time of the origin of life. The delivery of organics by asteroids, comets, and their fragments to the early Earth and other planetary bodies may have been an important source of the chemical ingredients required for life (Chyba & Sagan, 1992).

The soluble organic composition of carbonaceous chondrites (CCs) has been thoroughly investigated and a variety of organic compound classes have been found, including amino acids, amines, alcohols, aldehydes, ketones, polyols, and carboxylic acids (Burton, Stern, et al., 2012; Cronin et al., 1981; Ehrenfreund et al., 2001; Glavin et al., 2020; Kvenvolden et al., 1970; Pizzarello et al., 2004; Simkus et al., 2019). In particular, amino acids are prime targets in organic analyses of extraterrestrial materials because (1) amino acids are the monomers of proteins and may have been key to the

chemical evolution that led to the origin of life; (2) they are frequently found in a range of extraterrestrial samples, including various classes of meteorites and comet-exposed Stardust samples (Elsila et al., 2009, 2016, 2021); (3) the abundances, relative distributions, and enantiomeric and isotopic compositions of amino acids can be precisely measured to help establish the formation mechanisms and origins of these compounds (Simkus et al., 2019); and (4) there is sufficient structural diversity to probe parent body chemistry (Peltzer et al., 1984).

To illustrate (4) above, complex and diverse amino acid distributions can be indicative of asteroidal origins and exposure to parent body aqueous alteration (Aponte et al., 2015; Glavin et al., 2011). In contrast, cometary materials that may not have been exposed to extensive parent body aqueous alteration have so far revealed a much simpler amino acid distribution of glycine and possibly β-alanine (β-Ala; Altwegg et al., 2016; Elsila et al., 2009). Moreover, it has been shown that an amino acid distribution enriched in *n*-ω-amino acids (straight-chain, terminal amine) is often observed in meteorites that have experienced significant parent body thermal alteration (Burton, Elsila, et al., 2012; Burton et al., 2015). Furthermore, examining enantiomeric and isotopic compositions of amino acids in carbonaceous chondrites has revealed, in select cases, evidence of non-terrestrial L-enantiomeric excesses (L_{ee}) for some amino acids, providing important insights into the plausibility of abiotic chiral symmetry breaking mechanisms and a possible origin of biological homochirality on Earth (Cronin & Pizzarello, 1997; Elsila et al., 2016; Engel & Macko, 1997; Glavin et al., 2020; Glavin & Dworkin, 2009; Pizzarello & Cronin, 2000; Pizzarello et al., 2003). While meteoritic amino acid enantiomeric excesses have been observed in some meteorites, it is worth pointing out that racemic amino acids have also been detected in many meteorites. For example, nearly 50/50 D/L ratios for all tested chiral protein and non-protein amino acids in the Antarctic CM2 Yamato 791191 have been reported (Hamase et al., 2014); however, uncertainty estimates were not provided with these enantiomeric abundance estimates for the purpose of evaluating if the quantitated chiral amino acids were racemic within error. Other examples of the detection of racemic amino acids in various primitive Antarctic CR carbonaceous chondrites have also been reported (Glavin et al., 2011; Glavin & Dworkin, 2009; Martins, Alexander, et al., 2007).

As an alternative to making inferences about environments of unknown parent bodies via the analyses of CC chemical compositions, sample-return missions offer unique opportunities to explore the organic chemistry of known, small solar system bodies that have not been exposed to terrestrial weathering like most, if not all, fallen meteorites (Kvenvolden et al.,

2000). Sample-return missions also enable the analyses of these bodies using laboratory techniques not feasible to include on a spacecraft payload focused on in situ exploration. Despite the distinct advantages of analyzing returned samples, these materials are more challenging to obtain than meteorites, and consequently are typically less abundantly available than CCs.

The Japan Aerospace Exploration Agency (JAXA) Hayabusa mission was the first sample-return mission to collect and return asteroid materials to Earth. Hayabusa was launched in 2003 to near-Earth asteroid 25143 Itokawa, and returned particles to Earth in 2010. These particles were split up into four categories based on the compositions of the particles. For example, Category 2 particles are silicate-containing, while Category 3 particles are carbon-rich (https://curation.isas.jaxa.jp/curation/hayabusa/, accessed 22 February 2022).

A variety of research efforts have been undertaken to investigate the chemistry of Hayabusa particles. To illustrate, the chemistry of several Category 3 particles has been explored by others (Naraoka et al., 2015; Uesugi et al., 2014; Yabuta et al., 2014) in an attempt to determine the possible origins of these particles. Numerous microanalytical techniques, including scanning electron microscopy (SEM), nanosecondary ion mass spectrometry (NanoSIMS), and time-of-flight secondary ion mass spectrometry (ToF-SIMS), were implemented to study Category 3 particles and observed a combined lack of isotopic anomalies and chemical features different from those of meteoritic insoluble organic matter, suggesting the particles were unlikely to be extraterrestrial (Uesugi et al., 2014). A scanning transmission X-ray microscope using X-ray absorption near edge structure spectroscopy was applied to study additional Category 3 particles, which also resulted in the observation of a lack of isotopic anomalies, indicating the particles were not obviously of extraterrestrial origin (Yabuta et al., 2014). Furthermore, ToF-SIMS analyses identified a homogeneous carbon distribution in Category 3 particles that was seemingly associated with fluorine, nitrogen, and silicon, which is distinct from that observed in carbon-rich extraterrestrial samples, underscoring the possibility the particles were likely to be artifacts (Naraoka et al., 2015). Although these reports suggested contamination was a plausible source of Category 3 particles, neither of these studies were able to conclusively rule out the possibility of extraterrestrial origin, citing such evidence as isotopically normal compounds not being uncommon in extraterrestrial material, including micrometeorites and interplanetary dust particles (Messenger, 2000; Yabuta et al., 2013). Instead, it was emphasized that additional studies of the chemistry of Category 3 particles were needed (Yabuta et al., 2014), which would help to better ascertain the origin of Hayabusa particles.

There has only been one reported effort to explore the amino acid chemistry of Hayabusa particles, however. The amino acid analyses of dichloromethane/methanol extracts of two Category 2 Hayabusa particles (RA-QD02-0033 and RA-QD02-0049) were published in 2012 (Naraoka et al., 2012). The analyses were conducted using a very sensitive two-dimensional high-performance liquid chromatography with fluorescence detection technique that detected only glycine and alanine, but at abundances (glycine = 364 fmol; D,L-alanine = 105 fmol) similar to blank levels (glycine = 231 fmol, D,L-alanine = 76 fmol) with a correspondingly large alanine L_{ee} of ≈45%, and therefore were attributed to terrestrial contamination (Naraoka et al., 2012). Consequently, to date, it remains unclear if any other Hayabusa particles contain indigenous amino acids.

To address this absence in the literature, we have investigated the amino acid content of five Category 3 Hayabusa particles that have not previously been analyzed for amino acids, along with a grain of the CM2 Murchison meteorite (provided by Dr. Michael Zolensky from the NASA Johnson Space Center and stored in an N_2 cabinet prior to allocation). The assumption that Category 3 particles are the result of contamination is partially what motivated the current work. Since prior investigations (Naraoka et al., 2015; Uesugi et al., 2014; Yabuta et al., 2014) were unable to confirm the origin of Category 3 particles, a logical subsequent step to evaluate the provenance of Category 3 particles is to analyze their amino acid content. In this work, we used ultrahigh-performance liquid chromatography with fluorescence detection and time-of-flight mass spectrometry (LC-FD/ToF-MS) to study the amino acid content of Category 3 particles. The acid-hydrolyzed hot water extracts from these particles were analyzed to maximize the abundance of amino acids and thereby improve the chance of target analyte detection in these tiny samples.

MATERIALS AND METHODS

Particle Samples and Controls

Five Hayabusa particles were allocated by the JAXA Planetary Material Sample Curation Facility as part of its distribution for the 3rd International Announcement of Opportunity: RA-QD02-0012, RB-CV-0029, RB-CV-0080, RB-QD04-0052, and RA-QD02-0078 (Fig. 1), referred to as #12, #29, #80, #52, and #78, respectively. The particles, ranging in size from 83 to 100 μm in the longest dimension, were selected for the following reasons. (1) All were Category 3 grains (Chan et al., 2021; Ito et al., 2014; Kitajima et al., 2015; Yabuta et al., 2014) based on initial field emission

scanning electron microscopy (FE-SEM) with energy-dispersive X-ray spectrometer (EDX) characterization (Fig. S2 in the supporting information). (2) #80 contained signatures for elemental N, C, and O based on SEM-EDX analysis. (3) The particles were among the largest samples in the Hayabusa Category 3 collection. (4) #52 and #78 showed Raman features consistent with primitive unheated organic matter, which may be more likely to contain amino acids that would otherwise decompose at elevated temperatures (Ratcliff et al., 1974). All Hayabusa samples were kept in glass slides that were seated inside original sealed JAXA containers that were cleaned as described elsewhere (Yada et al., 2014), and stored in an ISO Class 5 cleanroom at the Open University. Prior to hot water extraction and acid hydrolysis, all samples were pressed into squares of baked gold foil to secure the particles during the execution of sample preparation protocols. A CM2 Murchison grain (≈200 μm prior to pressing into gold foil) and a baked gold foil procedural blank were extracted in parallel with the Hayabusa samples. The gold foil procedural blank and all sample handling tools were cleaned by baking at 500 °C in air for >10 h prior to use.

Details pertaining to the characteristics of the Hayabusa particles studied here can be found at the JAXA Hayabusa Curation website (https://curation.isas.jaxa.jp/curation/hayabusa/, accessed 22 February 2022), but will be briefly overviewed here. Particle #12 contained CO and FeS; #29 is a plagioclase particle composed of (C,O) and sodium chloride; #80 is comprised of (C,N,O), (C,O), aluminum, potassium, and silicone; #52 contains (C,F,O), aluminum, and titanium; and #78 is composed of CO, chloride, CFO, and magnesium. SEM data demonstrating these chemical compositions are shown in Fig. S2.

As both #52 and #78 exhibited clear organic signatures in their Raman spectra (see §1.2 of supporting information for more details), they were estimated to contain higher abundances of organic material on a per-grain basis and thus were pressed into their own respective squares of gold foil to allow for the amino acid analysis of their individual masses. Particles #12, #29, and #80 (referred to as #12,29,80) were all pressed into the same square of gold foil to allow for the amino acid analysis of their combined masses. An explanation for why these three particles were combined prior to analysis is provided in §1.2 of the supporting information. Sample and procedural blank properties are presented in Table 1. Additional details about the sample extraction and preparation procedures, as well as analytical conditions used for LC-FD/ToF-MS detection of amino acids in the samples, can be found in §1.2–1.3 of the supporting information.
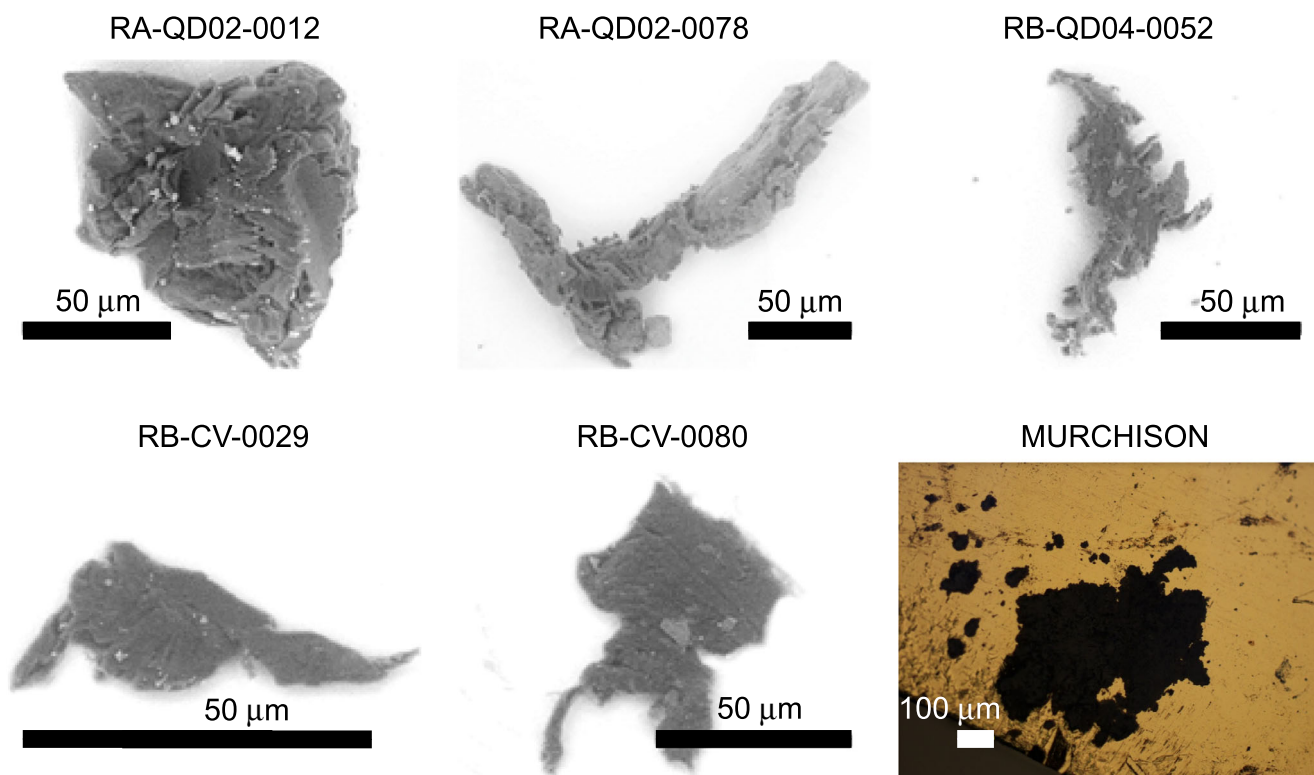
Fig. 1. Images of the five Hayabusa particles and one Murchison grain analyzed in this study. Backscattered electron images of the five allocated Hayabusa particles, obtained by SEM-EDX spectroscopy analysis at the Extraterrestrial Sample Curation Center of JAXA. Also included is a microphotograph of the Murchison grain studied here. In the Murchison grain image, the gold foil the grain has been pressed in is visible in the background.

RESULTS AND DISCUSSION

Amino Acid Results

Representative UV fluorescence chromatograms from LC analyses of an amino acid standard mixture, and the gold foil procedural blank, Murchison, and #12,29,80 extracts are shown in Fig. 2. Several peaks observed in the gold foil procedural blank extract that were identified as common amino acid contaminants, including L-enantiomers of protein amino acids, were also found in the Murchison and Hayabusa grain extracts, and thus were attributed to terrestrial contamination from the work-up procedure. The most abundant terrestrial contaminant was ε-amino-n-caproic acid (ε-ACA) (Fig. S5 in the supporting information), the hydrolysis product of nylon 6 and a common material used in clean rooms and laboratories (Dworkin et al., 2018). For more details on this contaminant and possible sources, see §2.2 of the supporting information. It should be emphasized that the presence of terrestrial contamination in the sample extracts did not prevent the detection and quantitation of amino acids at elevated abundances relative to background levels, as can be seen from the averaged, blank-corrected amino acid abundances reported in Table 2. Despite the primitive organic Raman signatures, #52 and #78 were largely depleted in amino acids, with peaks that were similar in intensity to those of the gold foil procedural blank. More details of the amino acid results for these two Hayabusa samples are provided in §2.2–2.3 of the supporting information. In contrast to #52 and #78, the acid-hydrolyzed hot water extracts of Murchison and #12,29,80 contained a suite of amino acids present at abundances above background levels.

The most prominent examples of amino acid detections that were likely to be indigenous to the samples were those of the non-protein amino acids, α-aminoisobutyric acid (α-AIB), β-Ala, β-aminoisobutyric acid (β-AIB), β-amino-n-butyric acid (β-ABA), and ɣ-amino-n-butyric acid (ɣ-ABA). Both #52 and #78 were found to contain a limited amino acid distribution, primarily comprised of low abundances (0.123 ± 0.002 nmol g^{-1} and 0.030 ± 0.001 nmol g^{-1}, respectively) of β-AIB. Both Murchison and #12,29,80 contained low abundances of β-AIB (0.16 ± 0.01 nmol g^{-1} and 0.31 ± 0.03 nmol g^{-1}, respectively) and β-ABA (0.048 ± 0.001 nmol g^{-1} and 0.090 ± 0.005 nmol g^{-1}, respectively).

Table 1. Measured masses of the gold foils and estimated masses of the Hayabusa particles and Murchison grain extracted for amino acid analyses in this study.

Specimens	Mass of gold foil used for each specimen (mg)	Total surface area of each pressed sample (μm^2)	Estimated masses of pressed samples (μg)[a,b]
Gold foil procedural blank	2.16	N/A	N/A
Murchison	4.41	238,464	3.82
#12,29,80	3.23	12,805	0.20
#52	2.49	8147	0.13
#78	3.03	21,362	0.34

[a]Masses were estimated based on an assumed flattened sample thickness of 5 μm and a specific gravity of 3.2 g cm^{-3} of the dominant mineral phases (forsterite and enstatite) of Itokawa. Despite these known dominant mineral phases of Itokawa, the dominant mineral phases of the Hayabusa particles studied here were not confirmed prior to analysis. To mitigate potential sample contamination or destruction using common techniques implemented when exploring mineralogy, such as SEM and electron probe microanalysis, the microparticles studied here were dedicated for amino acid analyses only. Consequently, the specific mineralogy of the particles studied here is not known in detail and is thus not thoroughly discussed here.

[b]Mass estimates were obtained by a three-step process. First, direct measurements of grain dimensions for each particle were made on an optical image to obtain the surface area of each pressed particle. Second, a flattened sample thickness of 5 μm was assumed and multiplied by the pressed particle surface area to deduce the particle volume. Third, the mass estimates were calculated via multiplying the particle volume by the specific gravity of 3.2 g cm^{-3}. Consequently, the accuracies of the particle mass estimates are dependent on the accuracies of the measured dimensions of each particle via optical imagery. To this end, the optical images were taken at 1280 × 960 pixels^2 at 20x magnification. At this magnification, the resolution was ≈ 0.5 μm pixel^{-1}. Furthermore, the specific gravity of 3.2 g cm^{-3} has been estimated for LLs (Wilkison & Robinson, 2000). Considering that Itokawa is compositionally similar to LL5 and LL6 chondrites, the specific gravity value used here is consistent with literature findings. In this work, we have also discussed the possibility that the particles might be derived from a C-type parent body, potentially a CR, and the specific gravity of 3.2 g cm^{-3} is also similar to this range of samples (e.g., Renazzo, 3.05 g cm^{-3}, Acfer 270, 3.26 g cm^{-3} [Macke et al., 2011]). Therefore, it remains plausible that the specific gravity values may be lower for some CCs (e.g., Al Rais and some CMs) in which case it is possible the actual masses for Category 3 (carbonaceous) grains could be lower. Under such a scenario, the particle masses given here would likely represent upper limit estimates.

It must be emphasized that neither β-AIB nor β-ABA was identified in the procedural blank (Fig. S7 in the supporting information) and these two non-protein amino acids were present as racemic (D≈L) or nearly racemic mixtures in the Hayabusa and Murchison samples within analytical errors (Table S4 in the supporting information).
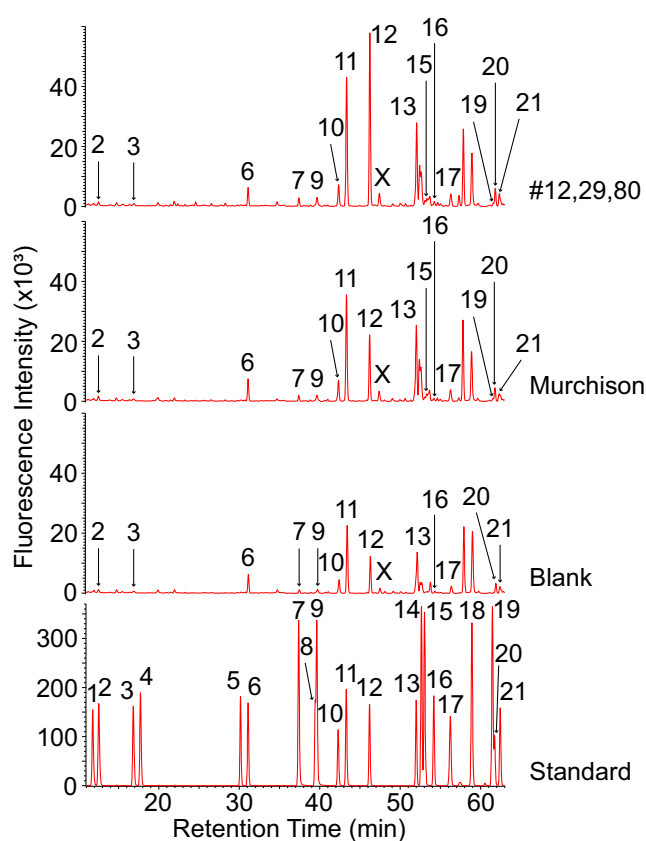

Fig. 2. Although contamination was observed, β-Ala (peak 12) was still found to be markedly larger in the #12,29,80 sample compared to the blank. The 11- to 63-min regions of the fluorescence chromatograms for a mixed amino acid standard, the procedural blank, Murchison, and #12,29,80. Analyte identifications are as follows: 1 = D-aspartic acid (D-Asp), 2 = L-Asp, 3 = L-glutamic acid (L-Glu), 4 = D-Glu, 5 = D-serine (D-Ser), 6 = L-Ser, 7 = D-isoserine (D-Ise), 8 = D-threonine (D-Thr), 9 = L-Ise, 10 = L-Thr, 11 = glycine (Gly), 12 = β-alanine (β-Ala), 13 = γ-amino-n-butyric acid (γ-ABA), 14 = D-β-aminoisobutyric acid (D-β-AIB), 15 = L-β-AIB, 16 = D-Ala, 17 = L-Ala, 18 = D-β-ABA, 19 = L-β-ABA, 20 = δ-aminovaleric acid (δ-AVA), 21 = α-AIB. Note: peak X is an unidentified compound with a primary amino group. (Color figure can be viewed at wileyonlinelibrary.com.)

Furthermore, it should be stressed that β-AIB and β-ABA are not common in natural samples, but have been detected above background levels in previous analyses of carbon-rich meteorites (Burton et al., 2014). There are select examples, however, of racemic β-ABA having been detected in natural terrestrial samples (Burton et al., 2011, 2014) that were dominated by biology and possibly influenced by industrial contamination. To evaluate the juxtaposition between racemic β-ABA detected in terrestrial samples and the particles analyzed here, it is helpful to compare the abundances of β-ABA relative to other amino acids found in terrestrial samples, with the same relative abundances in the particles analyzed here. In

Table 2. Summary of the averaged, blank-corrected abundances (nmol g^{-1}) of the C$_2$–C$_6$ amino acids in the acid-hydrolyzed (total) hot water extracts of the CM2 Murchison and Hayabusa particles analyzed here.

C#	Amine position	Amino acid	Murchison (Glavin et al., 2021), (0.08 g)	Murchison (present work) (3.82 µg)	#12,29,80 (0.20 µg)	#52 (0.13 µg)	#78 (0.34 µg)
2	α	Gly	40 ± 3	1.62 ± 0.04[a]	3.86 ± 0.05[a]	n.d.	n.d.
3	α	D-Ala	2.2 ± 0.01	0.03 ± 0.02	0.20 ± 0.06	n.d.	n.d.
3	α	L-Ala	3.0 ± 0.2	0.27 ± 0.02	0.41 ± 0.02	n.d.	n.d.
3	α	D-Ser	0.13 ± 0.03	n.d.	n.d.	n.d.	n.d.
3	α	L-Ser	3.5 ± 0.1	0.21 ± 0.01	n.d.	n.d.	n.d.
3	β	β-Ala	6.0 ± 0.2	1.49 ± 0.05	9.2 ± 0.3	n.d.	n.d.
3	β	D-Ise	N.R.	0.053 ± 0.004[a]	0.150 ± 0.005[a]	n.d.	n.d.
3	β	L-Ise	N.R.	0.083 ± 0.003[a]	0.22 ± 0.01[a]	n.d.	n.d.
4	α	D-Asp	0.59 ± 0.02	n.d.	n.d.	n.d.	n.d.
4	α	L-Asp	3.0 ± 0.1	0.05 ± 0.01[b]	0.02 ± 0.01[b]	n.d.	n.d.
4	α	D-Thr	0.02 ± 0.01	n.d.	n.d.	n.d.	n.d.
4	α	L-Thr	2.21 ± 0.05	0.546 ± 0.005	0.86 ± 0.04	n.d.	n.d.
4	α	D,L-α-ABA	2.0 ± 0.4	n.d.	n.d.	n.d.	n.d.
4	α	α-AIB	11.4 ± 0.5	0.21 ± 0.03	0.10 ± 0.01	n.d.	n.d.
4	β	D-β-ABA	1.8 ± 0.1	0.024 ± 0.001[c]	0.044 ± 0.005[c]	[f]	n.d.
4	β	L-β-ABA	1.6 ± 0.1	0.0246 ± 0.0004[c]	0.047 ± 0.002[c]	0.015 ± 0.001[c]	n.d.
4	β	D-β-AIB	2.4 ± 0.6[d]	0.085 ± 0.006[c]	0.16 ± 0.02[c]	0.062 ± 0.002[c]	0.0163 ± 0.0006[c]
4	β	L-β-AIB		0.07 ± 0.01[c]	0.14 ± 0.02[c]	0.060 ± 0.001[c]	0.0137 ± 0.0009[c]
4	γ	γ-ABA		2.07 ± 0.09	3.2 ± 0.2	n.d.	n.d.
5	α	D-Glu	1.03 ± 0.03	n.d.	n.d.	n.d.	n.d.
5	α	L-Glu	6.3 ± 0.1	0.010 ± 0.001[b]	0.04 ± 0.02[b]	n.d.	n.d.
5	α	D-Val	0.55 ± 0.02	n.d.	n.d.	n.d.	n.d.
5	α	L-Val	2.8 ± 0.1	0.51 ± 0.03[a]	0.69 ± 0.02[a]	0.06 ± 0.01	0.093 ± 0.005
5	α	D-Iva	10.0 ± 0.5	n.d.	n.d.	n.d.	n.d.
5	α	L-Iva	11.8 ± 0.7	n.d.	n.d.	n.d.	n.d.
5	α	D-Nva	0.1 ± 0.1	n.d.	n.d.	n.d.	n.d.
5	α	L-Nva	0.05 ± 0.03	n.d.	n.d.	n.d.	n.d.
5	β	S-3-APA	2.7 ± 0.1	n.d.	n.d.	n.d.	n.d.
5	β	R-3-APA		n.d.	n.d.	n.d.	n.d.
5	δ	δ-AVA	1.8 ± 0.1	0.39 ± 0.02[a]	0.96 ± 0.07[a]	n.d.	n.d.
6	α	D-Leu	N.R.	n.d.	n.d.	n.d.	n.d.
6	α	L-Leu	N.R.	n.d.	n.d.	0.07 ± 0.01[a]	0.064 ± 0.006
6	α	D-Ile	N.R.	n.d.	n.d.	n.d.	[f]
6	α	L-Ile	N.R.	n.d.	n.d.	0.021 ± 0.001[c]	0.0401 ± 0.0002
6	ε	ε-ACA	2.2 ± 0.6	n.d.[c,e]	n.d.[c,e]	n.d.[c,e]	n.d.[c,e]

For comparison, amino acid concentrations measured in the acid-hydrolyzed (total) hot water extract of a 0.08 g Murchison specimen (Glavin et al., 2021) are provided here. All data reported in the table from the current study are based on quantitation via optical fluorescence, except where noted by a superscript in the table (superscript definitions provided below). Blank corrections were performed by controlling for differences in surface areas of gold foils and derivatization volumes used between the procedural blank and the samples (see §1.3.1. of the supporting information for further details). Uncertainties (δ_x) reported here were calculated as the standard error $\left(\delta_x = \sigma_x \times (n)^{-1/2}\right)$ based on the standard deviation (σ_x) of the average values of triplicate ($n = 3$) measurements.

n.d. = Not determined because analyte abundance did not exceed blank levels.

N.R. = Analyte abundance not reported.

[a]Target analyte was tentatively detected by retention time and optical fluorescence, compared to an analytical standard. However, unambiguous identification of the target analyte was not confirmed because an unidentified analyte possessed an experimental accurate mass that overlapped with that of the target analyte, causing the measured experimental accurate mass of the target analyte to exceed the 10 parts per million (ppm) mass tolerance used. Consequently, the measurement of the target analyte did not experience interference via optical fluorescence, but did experience interference via accurate mass analysis. Therefore, abundances reported here are based on optical fluorescence and serve as upper limit estimates.

[b]Analyte was detected and quantitated via optical fluorescence, but was not detected by the mass spectrometer, due to inefficient ionization of the analyte in a heavily aqueous eluent composition.

[c]Quantitation of analytes was performed via ToF-MS due to interfering, optically fluorescent species that were fully resolved by accurate mass analysis.

[d]Analyte abundance was reported as the sum of abundances for γ-ABA + D,L-β-AIB because the analytes were not separated under the chromatographic conditions used.

[e]Measured sample ε-ACA abundances were <1.12 nmol, which was observed in the gold foil procedural blank.

[f]Unambiguous identification of the target analyte was not confirmed due to an unidentified analyte that coeluted with the target analyte via optical fluorescence and also possessed an experimental accurate mass that overlapped with that of the target analyte, causing the measured experimental accurate mass of the target analyte to exceed the 10 ppm mass tolerance used. Consequently, quantitation was not performed.

particular, comparing the abundances of β-ABA to common terrestrial contaminants, such as glycine and alanine, can help determine if the β-ABA detected in the particles is likely to have originated from a terrestrial source. To illustrate, if the β-ABA relative abundances in the particles are dissimilar from those of terrestrial samples, such a finding would indicate that the β-ABA detected in the particles is not likely to be the result of terrestrial processes. Although ε-ACA derived from nylon 6 was the most abundant amino acid contaminant in the Hayabusa sample extracts, nylon 6 does not contain β-ABA (Glavin et al., 2006), so nylon contamination is not a source of the elevated β-ABA in the Hayabusa samples. In addition, amino acid data from four terrestrial samples that can also be used for comparative purposes include soil samples from several meteorite fall sites in Murchison, Australia and Aguas Zarcas, Costa Rica (Glavin et al., 2021); Sutter's Mill, California (Burton et al., 2014); and Almahata Sitta, Sudan (Burton et al., 2011). The β-ABA/Gly ratio for Hayabusa material is 0.024 ± 0.001, while the same ratios for the Murchison, Aguas Zarcas, Sutter's Mill, and Almahata Sitta soils are <0.009, 0.0025 ± 0.0002, 0.004 ± 0.001, and 0.003 ± 0.001, respectively. Excluding the Murchison soil sample where β-ABA was not detected, the other soils possessed an average β-ABA relative abundance of 0.0032 ± 0.0003, which is $>7.5\times$ smaller than the β-ABA relative abundance of the Category 3 particles studied here. Similarly, the β-ABA/Ala ratio for the particles returned by Hayabusa is 0.15 ± 0.02, whereas the same ratios for the aforementioned soils are <0.015, 0.0038 ± 0.0004, 0.003 ± 0.001, and 0.006 ± 0.002, respectively. This equates to an average β-ABA/Ala ratio for the three terrestrial soils where β-ABA was detected of 0.0043 ± 0.0005, which is $\approx35\times$ smaller than the β-ABA relative abundance of the particles studied here. Consequently, the relative abundances of β-ABA detected in the Hayabusa particles analyzed in the current work are much higher than what is observed in terrestrial samples, suggesting that most of the β-ABA detected in the particles returned by the Hayabusa mission is plausibly extraterrestrial in origin. In the absence of dedicated Hayabusa contamination control witness materials available for amino acid analysis, these soils from four continents are the best available proxies for a range of plausible biological and industrial sources of amino acids. The amino acid analyses of the OSIRIS-REx spacecraft construction did not detect any β-ABA. Instead, the low levels of amino acid contamination were dominated by glycine (0.96–13.1 ng cm^{-2}) on different spacecraft surfaces (Dworkin et al., 2018) and were also inconsistent with the β-ABA/Gly ratios observed in the Hayabusa material. These combined observations of natural and industrial amino acid ratios provide additional supporting evidence

to suggest these analytes were not likely to be a result of terrestrial contamination imparted during sample handling.

Regarding additional non-protein amino acids of interest, Murchison had an elevated (≈2 times higher than background levels) abundance of γ-ABA, whose total abundance was 2.07 ± 0.09 nmol g^{-1}. Murchison also had an enhanced (≈3.4 times higher than background levels) abundance of α-AIB (total abundance = 0.21 ± 0.03 nmol g^{-1}). This observation is consistent with previous reports that α-AIB is among the more abundant non-protein amino acids in Murchison (Cronin & Pizzarello, 1983; Engel & Nagy, 1982; Glavin et al., 2021). The elevated abundances of α-AIB and γ-ABA in the Murchison grain extract, relative to blank levels (Fig. S11 in the supporting information), are a similar observation to that of a much larger Murchison sample mass that was extracted and analyzed for amino acids (Glavin et al., 2021). Such a similarity provides additional evidence that some portions of α-AIB and γ-ABA detected in the Murchison grain extract were likely derived from the particle itself. It is also worth noting that δ-aminovaleric acid (δ-AVA) was tentatively identified in the acid-hydrolyzed hot water extract of Murchison and #12,29,80, at lower abundances than other n-ω-amino acids (Table 2), similar to that observed in the analyses of larger quantities of Murchison (Glavin et al., 2021). It should be emphasized that such comparisons made here were done primarily for initial screening purposes, as opposed to verifying the absolute veracity of the amino acid abundances in the Murchison grain. To illustrate, comparing the analyses of a particle of Murchison to those of much larger samples of Murchison was executed simply to determine if the amino acid abundances and distributions observed in the Murchison particle were at all consistent with what would be expected of a Murchison sample based on previous literature reports. If not, this would indicate that the particle analyses performed here may not properly capture the amino acid content of the sample. However, since the comparison between the analytical results of the Murchison particle and that of larger Murchison samples was similar to a first approximation, this observation provided an indication that the particle analyses performed here were accurate and reliable.

Perhaps the most intriguing amino acid detection example in this work was that of β-Ala for #12,29,80 where β-Ala was ≈4.5 times more abundant than blank levels (Fig. 3), with a total abundance of 9.2 ± 0.3 nmol g^{-1}. To help evaluate the possibility that some of the β-Ala observed in the #12,29,80 extract may be of extraterrestrial origin, it is useful to compare the abundances of β-Ala in the sample and the blank,

relative to a common terrestrial protein amino acid contaminant, like alanine (Fig. 4). This comparison shows that the #12,29,80 β-Ala relative abundance is ≈2.5 times greater than that observed for the blank, and is thus sufficiently distinct from background levels to indicate that the presence of β-Ala in #12,29,80 is not due to contamination sources alone. To further assess the possibility that β-Ala may have originated from terrestrial sources, it is worth comparing the relative abundance of β-Ala to that of aspartic acid, a common terrestrial amino acid. To explain, it has previously been reported that β-Ala can be produced by the α-decarboxylation of aspartic acid (Peterson et al., 1997), and that another non-protein amino acid, γ-ABA, can be formed by the hydrolysis of 2-pyrrolidone, the pyrolysis product of glutamic acid (Lie et al., 2018; Vallentyne, 1964; Weiss et al., 2018). Thus, comparing the abundance of β-Ala relative to γ-ABA, to the abundance of aspartic acid relative to glutamic acid, can provide insight into the plausibility that the enlarged β-Ala abundance observed here may have been due to terrestrial amino acid contamination and subsequent degradation. For the #12,29,80 sample, the β-Ala/γ-ABA ratio is 2.9 ± 0.2 and the Asp/Glu ratio is 0.5 ± 0.4. If these two ratios were similar to each other, that would suggest β-Ala was likely derived from aspartic acid. However, since these two ratios are clearly distinct from one another, this finding indicates that the elevated levels of β-Ala in the #12,29,80 sample are unlikely to be caused by the degradation of common terrestrial contaminant amino acids like aspartic acid, alone. Therefore, the combination of four different and consistent abundance characteristics associated with β-Ala in the #12,29,80 sample indicated that a portion of the β-Ala in the acid-hydrolyzed hot water extract must have been derived from the sample itself, and not contamination from the processing procedures. These characteristics include (1) enhanced total abundance, (2) enlarged abundance relative to blank levels, (3) heightened relative abundances compared to common terrestrial contaminants (e.g., glycine [Fig. S12 in the supporting information] and alanine [Figs. 4, S13, and S14]), and (4) distinct relative abundance compared to that of aspartic acid, a potential terrestrial source of β-Ala.

In addition to measuring amino acid concentrations and relative abundances, enantiomeric ratios and L_{ee} of select chiral amino acids were also determined (Table S4). As noted previously, β-ABA was racemic for Murchison and the #12,29,80 grains, as was β-AIB for #12,29,80 and #52 (Table S4). However, β-AIB was found to be slightly enriched in the D-enantiomer for the Murchison grain ($L_{ee} = -7.5 \pm 7.0\%$) and #78 ($L_{ee} = -8.7 \pm 4.2\%$) as indicated by their negative L-enantiomeric excess percentage values that lie just

outside of analytical errors (Table S4). Similar, comparatively large abundance estimates of D-β-AIB versus L-β-AIB were reported for Murchison by Koga and Naraoka (2017), although these abundance estimates were accompanied by significant uncertainty estimates due to chromatographic interference that was observed. Nonetheless, given the very low concentrations of β-AIB in these Murchison and Hayabusa grain extracts, and their associated relatively large % L_{ee} uncertainties, the small D-β-AIB enantiomeric excesses should be interpreted with caution. Similarly, enantiomeric measurements of isoserine (Ise) for Murchison and #12,29,80 appeared to possess relatively large L_{ee} values of ≈20% (Table S4), yet it is important to bear in mind that Ise was only tentatively observed at low abundances, which warrants cautious evaluation of Ise enantiomeric excesses as well. Compound-specific stable isotope measurements (Elsila et al., 2009) of the individual D- and L-enantiomers are necessary to firmly establish a non-terrestrial origin of any measured enantiomeric excess. However, due to limited sample mass and low amino acid abundances, isotopic measurements were not feasible here. Future improvements in compound-specific stable isotope measurement technologies for amino acids will be needed to more rigorously evaluate the source of the enantiomeric excesses in these samples.

Comparison to Previous Itokawa Analyses

Naraoka et al. (2012) reported on the amino acid analyses of two Itokawa particles, which revealed that only glycine and D,L-alanine were detected in the procedural blanks and each of the grains. Extracts of RA-QD02-0033 showed glycine and alanine did not exceed blank levels and RA-QD02-0049 contained low levels of glycine, D-alanine, and L-alanine slightly greater than those observed for the procedural blanks (≈1.6, ≈1.3, and ≈1.4 times higher, respectively, than blank levels). Reasonably, it was concluded that glycine and D,L-alanine were largely due to contamination (Naraoka et al., 2012). In the current study, however, we observed a much broader distribution of amino acids in the Hayabusa grain extracts, including two terrestrially rare non-protein amino acids that are not common terrestrial contaminants.

The contrast in amino acid results between the present work and Naraoka et al. may be because the Category 3 particles analyzed here were carbon-rich and contained more organic material than the Category 2 particles analyzed by Naraoka et al. (2012). It is also possible that the dissimilar amino acid results might partially be due to differences in sample preparation protocols. Hot water extraction at 100 °C for 24 h was used in this study,
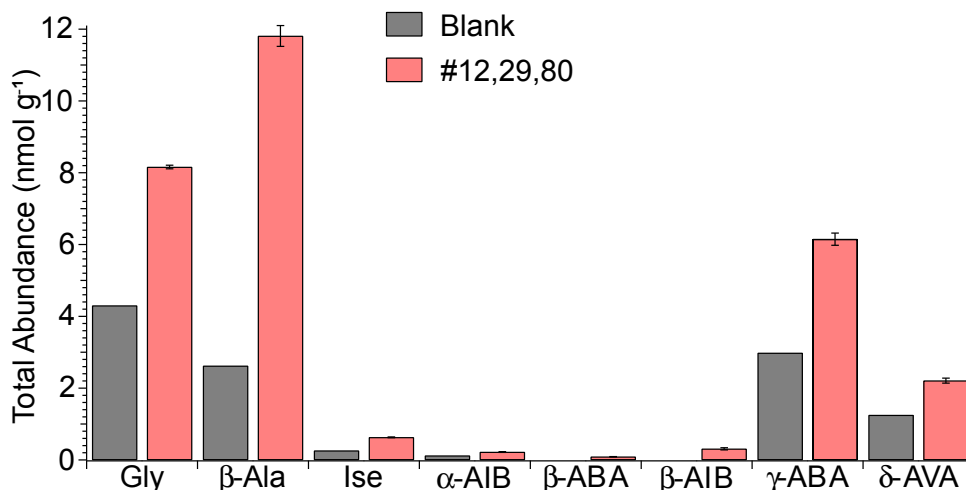
Fig. 3. The comparatively large abundance of β-Ala in the #12,29,80 sample relative to the procedural blank strongly suggests a sample contribution. Blank-uncorrected total abundances of select non-protein amino acids and glycine observed in the #12,29,80 sample compared to their corresponding blank levels. Multiple amino acids were observed above background levels in the #12,29,80 sample with β-Ala being the most abundant. Both β-AIB and β-ABA were identified in the Hayabusa grains, but were not present in the blank. The standard errors reported here were taken from Table 2. Note: Uncertainties of blank abundances are not shown because replicate blank measurements were not made. However, replicate measurements of other laboratory blanks have indicated that background amino acid abundance estimates were not accompanied by large uncertainty estimates.
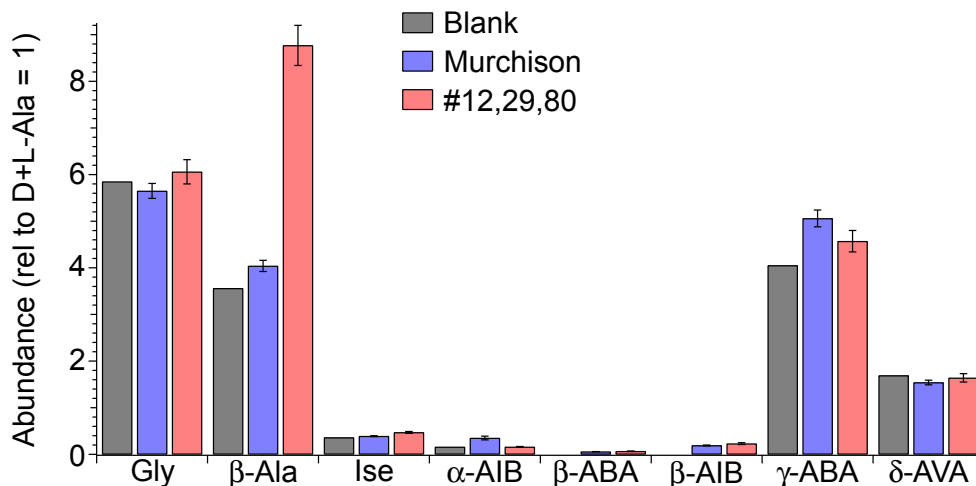

Fig. 4. The enhanced relative abundance of β-Ala in #12,29,80 is distinct from that observed in the blank and therefore supports the hypothesis that a portion of this non-protein amino acid is derived from the sample. Blank-uncorrected relative abundances of select non-protein amino acids and glycine observed for Murchison and #12,29,80. Sample relative abundances are compared to those of the procedural blank to distinguish which analyte relative abundances are inconsistent with background levels, and are therefore likely to have been contributed by the sample. The standard errors reported here were based on the average values and associated standard errors reported in Table 2, and propagated through the appropriate equations. Uncertainties of blank relative abundances are not available because of reasons stated in the Fig. 3 legend.

whereas Naraoka et al. (2012) rinsed the particle surfaces with a small volume (≈0.6 μL) of 50:50 dichloromethane/methanol for ≈10 s without applying heat (Naraoka, personal communication). This less aggressive organic extraction approach was chosen because a heated, aqueous extraction protocol would have interfered with planned, downstream mineral analyses by imparting aqueous weathering to the particles' mineral content (Naraoka et al., 2012). It is plausible the aqueous extraction protocol used in the current study, which entailed a comparatively large extraction volume (500 μL) at an elevated temperature (100 °C) over a long (24-h) time span (Glavin et al., 1999), provided for more efficacious amino acid extraction.

Comparison to Other Chondrites

Remote sensing (Abe et al., 2006; Okada et al., 2006) and mineral (Brady & Cherniak, 2010; Huss et al., 2006) data indicate that Itokawa is compositionally similar to LL5 and LL6 ordinary chondrites (OCs). Therefore, comparing published OC amino acid data to those of Hayabusa grains may elucidate if the observed Hayabusa amino acid distribution is consistent with a typical amino acid distribution for representative meteorites. Likely due to the depleted amino acid abundances in OCs, there are few reports of OC amino acids published (Botta et al., 2008; Burton et al., 2011; Chan et al., 2012, 2018; Jenniskens et al., 2014; Martins, Hofmann, et al., 2007). To our knowledge, there are no reports of LL6 OCs and one report with three LL5 OCs: LaPaz Icefield (LAP) 03573, LAP 03624, and LAP 03637 (Botta et al., 2008). These LL5 OCs contained amino acid profiles comprised only of glycine, β-Ala, and ɣ-ABA at abundances ranging from 0.04 to 0.13 nmol g^{-1}. Similar to the LL5s, glycine, β-Ala, and ɣ-ABA were also the most abundant in #12,29,80 analyzed in the current study. Given the uncertainties in relative amounts of glycine contamination between these LL5s, and the #12,29,80 sample analyzed in the current work, comparing the abundances of β-Ala and ɣ-ABA among these samples could be a more useful measurement by which to glean information about possible parent body conditions and syntheses that contributed to observed non-protein amino acid abundances, as opposed to comparing abundances of non-protein amino acids to glycine. When performing such a comparison, it was found that the #12,29,80 sample contained a ≈6.2–8.0 times greater β-Ala/ɣ-ABA ratio than the LL5s (Fig. 5). Consequently, the amino acid relative abundances observed in #12,29,80 appear to be distinct from those of LL5 OCs.

In addition to mineralogical similarities with LL5s, it has been reported that Itokawa organic content may have been influenced by the infall of primitive material from CR chondrites (Chan et al., 2021), which contain a greater diversity of amino acids (Glavin et al., 2011) than LL5s. To illustrate, NanoSIMS analysis of the hydrogen, as a proxy for water content, in Itokawa silicates has revealed that Itokawa was likely rehydrated by exogenous delivery of water, perhaps from CR chondrites (Chan et al., 2021). Therefore, it is worth exploring if the β-Ala/ɣ-ABA ratio of #12,29,80 is similar to that of primitive, carbon-rich CRs to evaluate the likelihood that the amino acids of #12,29,80 may also have been affected by the infall of water-rich CCs. For this purpose, the β-Ala/ɣ-ABA ratio of the #12,29,80 sample was compared to that of weakly altered (petrologic type >2.5) and more

aqueously altered (petrologic type <2.5) CR chondrites. The weakly altered CR chondrites used for this comparison were CR2.7 Graves Nunataks (GRA) 95229 (Martins, Hofmann, et al., 2007), CR2.7 Miller Range (MIL) 090657 (Aponte et al., 2020), and CR2.8 Queen Alexandria Range (QUE) 99177 and CR2.8 Elephant Moraine (EET) 92042 (Glavin et al., 2011). The more aqueously altered CR chondrites used for this comparison were CR 2.0 Grosvenor Mountains (GRO) 95577 (Glavin et al., 2011) and CR2.4 MIL 090001 (Aponte et al., 2020). The weakly altered CR2s contained β-Ala/ɣ-ABA ratios of only ≈41–64% of that quantitated for #12,29,80, whereas those for more aqueously altered CR2s were ≈82–113% of that observed for #12,29,80 (Fig. 5). Furthermore, it can be seen that the total amino acid abundance for #12,29,80 (20.3 ± 0.4 nmol g^{-1}) is concomitantly similar to those (≈17–20 nmol g^{-1}) of more aqueously altered CRs, and contrasts with those (up to ≈3000 nmol g^{-1}) of weakly altered CRs (Fig. 5). The combined similarities of the dual amino acid characteristics (i.e., β-Ala/ɣ-ABA ratio and total amino acid abundance) between #12,29,80 and more aqueously altered CRs are intriguing to note. Further evaluations of such comparisons during future Itokawa analyses will be important to better assess the plausibility that the amino acid content of Itokawa may have been influenced by exogenous delivery from water-rich chondrites.

Despite similar mineralogical features, differences in amino acid distribution and abundances between these Hayabusa grains and Antarctic LL5 OCs could indicate the Category 3 grains returned by Hayabusa may have originated from another, more carbon-rich parent body. This interpretation is in line with the observation of a 6 m xenolithic black boulder on the surface of Itokawa, which was suggested to be a carbonaceous chondrite originated from an impactor that was 200–800 m in diameter (Chan et al., 2021; Nagaoka et al., 2014). It was also concluded that traces of exogenous material may exist on Itokawa as evidenced by the presence of both primitive and processed organic material within a single Itokawa grain, due to spectral and isotopic similarities to carbon-rich CR carbonaceous chondrites and interplanetary dust particles rather than OCs (Chan et al., 2021). Additionally, a recent SEM-EDX analysis of Itokawa material found evidence of exogenous copper sulfide in the form of a cubanite–chalcopyrite–troilite–pyrrhotite assemblage, the components of which are emblematic of low-temperature, aqueous alteration and more consistent with CI, R, or CK chondrites, as opposed to LL OC-type material akin to that of asteroid Itokawa (Burgess & Stroud, 2021). It is worth noting that DellaGiustina et al. (2021) reported Vestoid-like xenoliths on the surface of asteroid 101955 Bennu
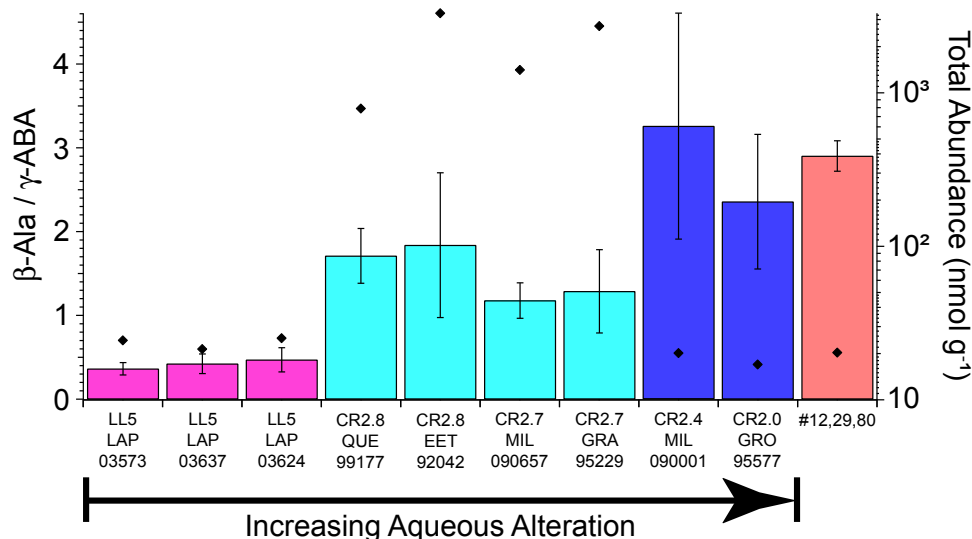
Fig. 5. The β-Ala/ɣ-ABA ratio in #12,29,80 is inconsistent with those observed in LL5 OCs and fits some CRs, but not others. The left axis shows the blank-corrected abundance of β-Ala, relative to ɣ-ABA, observed in #12,29,80 and previously analyzed thermally altered LL5 OCs (Botta et al., 2008), more thermally altered CR2s (Aponte et al., 2020; Glavin et al., 2010; Martins, Hofmann, et al., 2007), and more aqueously altered CR2s (Aponte et al., 2020; Glavin et al., 2011). Petrologic subtypes for CR2 chondrites were taken from elsewhere (Harju et al., 2014) for GRO 95577, MIL 090001, GRA 95229, and QUE 99177, and from Aponte et al. (2020) for MIL 090657 and EET 92042. The right axis demonstrates the total amino acid abundances (black diamonds) in the respective samples. The standard error reported here for the β-Ala/ɣ-ABA ratio was based on the average values and associated standard errors reported in Table 2, and propagated through the appropriate equations. All other uncertainty estimates shown here were obtained from their respective literature sources.

from in situ observations by the NASA OSIRIS-REx spacecraft. It is possible that such xenolithic material may be found in the OSIRIS-REx sample.

Aside from the possibility of exogenous delivery affecting the organic content of Hayabusa particles, it is possible that the observed amino acid abundances and distributions may be the product of an unusual contamination that is not easily explained by the biology of obvious industrial materials, as the species of primary interest in this study are dissimilar from that which would be expected from biological or industrial contamination. To evaluate such a possibility, comparisons to witness coupons would be beneficial, as has been emphasized previously in the literature (Uesugi et al., 2014; Yabuta et al., 2014). However, Hayabusa lacked flight witness materials; thus, we relied on the distribution and relative abundances of amino acids to discriminate between terrestrial and extraterrestrial origins. The amino acid analyses performed here help to address this need, and the resultant data present evidence to suggest some compounds may have an extraterrestrial origin.

The detection of amino acids in thermally altered asteroid material is nonetheless curious, as thermally altered chondrites were reported to be amino acid poor (Cronin & Moore, 1971, 1976; Glavin et al., 2010). Yet, it is not unfounded for thermally altered material to

contain amino acids. To illustrate, low abundances of amino acids were found in the thermally altered Almahata Sitta ureilite (Burton et al., 2011; Glavin et al., 2010; Herrin et al., 2010; Zolensky et al., 2010), and n-ω-amino acids, including β-Ala, were abundant in thermally altered CV and CO chondrites (Burton, Elsila, et al., 2012). Comparatively large abundances of n-ω-amino acids like glycine, β-Ala, and ɣ-ABA observed for #12,29,80 are consistent with previous amino acid studies of thermally altered CCs (Burton, Elsila, et al., 2012) and could highlight the potential importance of alternative amino acid formation mechanisms, such as mineral-catalyzed Fischer Tropsch/Haber Bosch-type reactions that may have been prominent in numerous solar system environments (Anders et al., 1973; Levy et al., 1973; Studier et al., 1968). However, the presence of β-AIB and a high β-Ala/ɣ-ABA ratio was not similarly observed in thermally altered CV and CO carbonaceous chondrites, which suggests the involvement of low-temperature aqueous activity may also contribute to amino acid synthesis in Hayabusa material.

Potential Particle Origins and Associated Implications

Given the extremely small masses of Hayabusa samples available for amino acid analysis, and the sensitive nature of such samples to amino acid

contamination, performing a thorough investigation of particle mineralogy prior to amino acid analysis was not feasible. Doing so would have likely resulted in sample loss or contamination, which would have compromised the scientific integrity of the samples for amino acid analysis. However, there was one particle for which some mineralogical information was available based on initial SEM-EDX analysis, and that was particle #29. Plagioclase was observed in particle #29 upon SEM-EDX analysis performed by the JAXA curation team. Plagioclase is a mineral that has been observed in a variety of CCs and OCs, including CR chondrites (Tenner et al., 2019), CV chondrites (Krot et al., 2002), and type 5 and 6 OCs (Huss et al., 2006; Van Schmus & Wood, 1967). In OCs, plagioclase has been observed as a primary phase (Lewis et al., 2022). Given the ubiquity of plagioclase, the presence of this mineral in particle #29 is not a selective feature for the purpose of constraining a range of possible parent bodies. To investigate the possible origin of the microparticles studied here, namely #29, quantitative SEM-EDX data of these Hayabusa samples was obtained from the JAXA curation team. For particle #29, primary chemical elements that make up plagioclase were observed, such as Na, Al, Si, and O, although these elements tended to be minor components based on quantitative SEM-EDX data. This pattern was similarly observed in the other Hayabusa particles analyzed here, whereby elemental components of the particles that could otherwise help glean possible mineral phase composition within these grains, and in turn aid in assessing the origins of these samples, were relatively low in abundance. In contrast, C was relatively large in abundance in all five Hayabusa grains analyzed here. Given the quantitative SEM-EDX data collected for these particles, it is not possible to adequately constrain the range of parent bodies these grains may have originated from. This matter is complicated by the fact that the grain masses were too small to obtain isotopic data for these samples, which is a very useful analytical tool for determining the origins of samples.

Although the particle origins cannot be deduced based on the SEM-EDX data, it is useful to evaluate how different plausible particle origins would affect the implications of this work, within the context of the amino acid data collected here. The first possible scenario is that the Hayabusa particles analyzed here were collected from the surface of asteroid Itokawa. If so, the amino acid data observed here would indicate that non-protein amino acids, such as β-Ala, β-AIB, and β-ABA, represent extraterrestrial amino acids recovered from the surface of asteroid Itokawa. Furthermore, it is possible that these amino acids may have originated from exogenous material delivered to the Itokawa asteroid surface from a more carbon-rich source. The second possible scenario is

that the particles did not originate from asteroid Itokawa and instead were derived from an unknown terrestrial source. Given the lack of available Hayabusa flight witness materials that experienced the same environments as the samples collected at Itokawa, it is difficult to rule out the possibility that the non-protein amino acids detected in the returned Hayabusa grains were derived from a highly unusual and unknown terrestrial contamination source.

CONCLUSIONS

The results of this work serve as the first evidence of plausibly extraterrestrial, non-protein amino acids in asteroid material obtained from a sample-return mission. Due to the finite sample masses available for study and the small quantities of amino acids extracted from the grains, compound-specific stable isotopic measurements necessary to make definitive conclusions regarding the specific provenance of these non-protein amino acids and the origins of the measured enantiomeric excesses (Elsila et al., 2009) were not possible. Therefore, isotopic measurements of the amino acid content of Hayabusa material using more sensitive stable isotopic analyses than are currently available, and comparisons with other carbon-rich meteorites and samples returned from Ryugu and Bennu, will be vital to better assess the exact origins of the non-protein amino acids in the Hayabusa grains analyzed here.

Despite similarities between Itokawa and thermally altered LL5 and LL6 OCs (Abe et al., 2006; Brady & Cherniak, 2010; Huss et al., 2006; Okada et al., 2006), the Hayabusa amino acid content observed here was dissimilar to thermally altered OCs (Botta et al., 2008), but preliminarily analogous to more aqueously altered CR2s. This underscores the possibility that materials may have transported between small solar system bodies to contribute to the chemistry of sample-return mission target asteroids (Chan et al., 2021). Through the use of very sensitive and selective analytical techniques, such as the methods described here, discoveries similar to those detailed in this work highlight the power of sample-return missions like Hayabusa2 and OSIRIS-REx to unveil new insights into organic synthesis in the solar system and thereby uncover important implications for the origin of life on Earth and possibly elsewhere.

Data Availability Statement—The data that support the findings of this study are openly available in the NASA PubSpace archive at https://www.ncbi.nlm.nih.gov/pmc/funder/nasa/. The data that support the findings of this study are also available in the supplementary material of this article.

Editorial Handling—Dr. Scott Sandford

REFERENCES

Abe, M., Takagi, Y., Kitazzato, K., Abe, S., Hiroi, T., Vilas, F., Clark, B. E. et al. 2006. Near-Infrared Spectral Results of Asteroid Itokawa from the Hayabusa Spacecraft. *Science* 312: 1334–8.

Altwegg, K., Balsiger, H., Bar-Nun, A., Berthelier, J.-J., Bieler, A., Bochsler, P., Briois, C. et al. 2016. Prebiotic Chemicals—Amino Acid and Phosphorus—in the Coma of Comet 67P/Churyumov-Gerasimenko. *Science Advances* 2: 1.

Anders, E., Hayatsu, R., and Studier, M. H. 1973. Organic Compounds in Meteorites. *Science* 182: 781–90.

Aponte, J. C., Dworkin, J. P., and Elsila, J. E. 2015. Indigenous Aliphatic Amines in the Aqueously Altered Orgueil Meteorite. *Meteoritics & Planetary Science* 50: 1733–49.

Aponte, J. C., Elsila, J. E., Hein, J. E., Dworkin, J. P., Glavin, D. P., McLain, H. L., Parker, E. T., Cao, T., Berger, E. L., and Burton, A. S. 2020. Analysis of Amino Acids, Hydroxy Acids and Amines in CR Chondrites. *Meteoritics & Planetary Science* 55: 2422–39.

Botta, O., Martin, Z., Emmenegger, C., Dworkin, J. P., Glavin, D. P., Harvey, R. P., Zenobi, R., Bada, J. L., and Ehrenfreund, P. 2008. Polycyclic Aromatic Hydrocarbons and Amino Acids in Meteorites and Ice Samples from LaPaz Icefield, Antarctica. *Meteoritics & Planetary Science* 43: 1465–80.

Brady, J. B., and Cherniak, D. J. 2010. Diffusion in Minerals: An Overview of Published Experimental Diffusion Data. In *Diffusion in Minerals and Melts*, edited by Y. Zhang and D. J. Cherniak, 899–920. Chantilly, Virginia: The Mineralogical Society of America.

Burgess, K. D., and Stroud, R. M. 2021. Exogenous Copper Sulfide in Returned Asteroid Itokawa Regolith Grains Are Likely Relicts of Prior Impacting Body. *Communications Earth & Environment* 2.

Burton, A. S., Elsila, J. E., Callahan, M. P., Martin, M. G., Glavin, D. P., Johnson, N. M., and Dworkin, J. P. 2012. A Propensity for *n*-ω-Amino Acids in Thermally Altered Antarctic Meteorites. *Meteoritics & Planetary Science* 47: 374–86.

Burton, A. S., Glavin, D. P., Callahan, M. P., Dworkin, J. P., Jenniskens, P., and Shaddad, M. H. 2011. Heterogeneous Distributions of Amino Acids Provide Evidence of Multiple Sources Within the Almahata Sitta Parent Body, Asteroid 2008 TC3. *Meteoritics & Planetary Science* 46: 1703–12.

Burton, A. S., Glavin, D. P., Elsila, J. E., Dworkin, J. P., Jenniskens, P., and Yin, Q.-Z. 2014. The Amino Acid Composition of the Sutter's Mill CM2 Carbonaceous Chondrite. *Meteoritics & Planetary Science* 49: 2074–86.

Burton, A. S., McLain, H. L., Glavin, D. P., Elsila, J. E., Davidson, J., Miller, K. E., Andronikov, A. V., Lauretta, D., and Dworkin, J. P. 2015. Amino Acid Analyses of R and CK Chondrites. *Meteoritics & Planetary Science* 50: 470–82.

Burton, A. S., Stern, J. C., Elsila, J. E., Glavin, D. P., and Dworkin, J. P. 2012. Understanding Prebiotic Chemistry Through the Analysis of Extraterrestrial Amino Acids and Nucleobases in Meteorites. *Chemical Society Reviews* 41: 5459–72.

Chan, Q. H. S., Martins, Z., and Sephton, M. A. 2012. Amino Acid Analyses of Type 3 Chondrites Colony, Ornans, Chainpur, and Bishunpur. *Meteoritics & Planetary Science* 47: 1502–16.

Chan, Q. H. S., Stephant, A., Franchi, I. A., Zhao, X., Brunetto, R., Kebukawa, Y., Noguchi, T. et al. 2021. Organic Matter and Water from Asteroid Itokawa. *Scientific Reports* 11: 5125.

Chan, Q. H. S., Zolensky, M. E., Kebukawa, Y., Fries, M., Ito, M., Steele, A., Rahman, Z. et al. 2018. Organic Matter in Extraterrestrial Water-Bearing Salt Crystals. *Science Advances* 4: eaao3521.

Chyba, C., and Sagan, C. 1992. Endogenous Production, Exogenous Delivery and Impact-Shock Synthesis of Organic Molecules: An Inventory for the Origins of Life. *Nature* 355: 125–32.

Cronin, J. R., Gandy, W. E., and Pizzarello, S. 1981. Amino-Acids of the Murchison Meteorite: I. Six Carbon Acyclic Primary Alpha-Amino Alkanoic Acids. *Journal of Molecular Evolution* 17: 265–72.

Cronin, J. R., and Moore, C. B. 1971. Amino Acid Analyses of the Murchison, Murray, and Allende Carbonaceous Chondrites. *Science* 172: 1327–9.

Cronin, J. R. and Moore, C. B. 1976. Amino Acids of the Nogoya and Mokoia Carbonaceous Chondrites. *Geochimica et Cosmochimica Acta* 40: 853–7.

Cronin, J. R., and Pizzarello, S. 1983. Amino Acids in Meteorites. *Advances in Space Research* 3: 5–18.

Cronin, J. R., and Pizzarello, S. 1997. Enantiomeric Excesses in Meteoritic Amino Acids. *Science* 275: 951–5.

DellaGiustina, D. N., Kaplan, H. H., Simon, A. A., Bottke, W. F., Avdellidou, C., Delbo, M., Ballouz, R.-L. et al. 2021. Exogenic Basalt on Asteroid (101955) Bennu. *Nature Astronomy* 5: 31–8.

Dworkin, J. P., Adelman, L. A., Ajluni, T., Andronikov, A. V., Aponte, J. C., Bartels, A. E., Beshore, E. et al. 2018. OSIRIS-REx Contamination Control Strategy and Implementation. *Space Science Reviews* 214: 19.

Ehrenfreund, P., Glavin, D. P., Botta, O., Cooper, G., and Bada, J. L. 2001. Extraterrestrial Amino Acids in Orgueil and Ivuna: Tracing the Parent Body of CI Type Carbonaceous Chondrites. *Proceedings of the National Academy of Sciences* 98: 2138–41.

Elsila, J. E., Aponte, J. C., Blackmond, D. G., Burton, A. S., Dworkin, J. P., and Glavin, D. P. 2016. Meteoritic Amino Acids: Diversity in Compositions Reflects Parent Body Histories. *ACS Central Science* 2: 370–9.

Elsila, J. E., Glavin, D. P., and Dworkin, J. P. 2009. Cometary Glycine Detected in Samples Returned by Stardust. *Meteoritics & Planetary Science* 44: 1323–30.

Elsila, J. E., Johnson, N. M., Glavin, D. P., Aponte, J. C., and Dworkin, J. P. 2021. Amino Acid Abundances and Compositions in Iron and Stony-Iron Meteorites. *Meteoritics & Planetary Science* 56: 586–600.

Engel, M., and Macko, S. 1997. Isotopic Evidence for Extraterrestrial Non-Racemic Amino Acids in the Murchison Meteorite. *Nature* 389: 265–8.

Engel, M. H., and Nagy, B. 1982. Distribution and Enantiomeric Composition of Amino Acids in the Murchison Meteorite. *Nature* 296: 837–40.

Glavin, D. P., Aubrey, A. D., Callahan, M. P., Dworkin, J. P., Elsila, J. E., Parker, E. T., Bada, J. L., Jenniskens, P., and Shaddad, M. H. 2010. Extraterrestrial Amino Acids in the Almahata Sitta Meteorite. *Meteoritics & Planetary Science* 45: 1695–709.

Glavin, D. P., Bada, J. L., Brinton, K. L. F., and McDonald, G. D. 1999. Amino Acids in the Martian Meteorite Nakhla. *Proceedings of the National Academy of Sciences* 96: 8835–8.

Glavin, D. P., Burton, A. S., Elsila, J. E., Aponte, J. C., and Dworkin, J. P. 2020. The Search for Chiral Asymmetry As a Potential Biosignature in Our Solar System. *Chemical Reviews* 120: 4660–89.

Glavin, D. P., Callahan, M. P., Dworkin, J. P., and Elsila, J. E. 2011. The Effects of Parent Body Processes on Amino Acids in Carbonaceous Chondrites. *Meteoritics & Planetary Science* 45: 1948–72.

Glavin, D. P., and Dworkin, J. P. 2009. Enrichment of the Amino Acid L-Isovaline by Aqueous Alteration on CI and CM Meteorite Parent Bodies. *Proceedings of the National Academy of Sciences* 106: 5487–92.

Glavin, D. P., Dworkin, J. P., Aubrey, A., Botta, O., Doty, J. H., Martins, Z., and Bada, J. L. 2006. Amino Acid Analyses of Antarctic CM2 Meteorites Using Liquid Chromatography-Time of Flight-Mass Spectrometry. *Meteoritics & Planetary Science* 41: 889–902.

Glavin, D. P., Elsila, J. E., McLain, H. L., Aponte, J. C., Parker, E. T., Dworkin, J. P., Hill, D. H., Connolly Jr., H. C., and Lauretta, D. S. 2021. Extraterrestrial Amino Acids and L-Enantiomeric Excesses in the CM2 Carbonaceous Chondrites Aguas Zarcas and Murchison. *Meteoritics & Planetary Science* 56: 148–73.

Hamase, K., Nakauchi, Y., Miyoshi, Y., Koga, R., Kusano, N., Onigahara, H., Naraoka, H. et al. 2014. Enantioselective Determination of Extraterrestrial Amino Acids Using a Two-Dimensional Chiral High-Performance Liquid Chromatographic System. *Chromatography* 35: 103–10.

Harju, E. R., Rubin, A. E., Ahn, I., Choi, B.-G., Ziegler, K., and Wasson, J. T. 2014. Progressive Aqueous Alteration of CR Carbonaceous Chondrites. *Geochimica et Cosmochimica Acta* 139: 267–92.

Herrin, J. S., Zolensky, M. E., Ito, M., Le, L., Mittlefehldt, D. W., Jenniskens, P., Ross, A. J., and Shaddad, M. H. 2010. Thermal and Fragmentation History of Ureilitic Asteroids: Insights from the Almahata Sitta Fall. *Meteoritics & Planetary Science* 45: 1789–803.

Huss, G. R., Rubin, A. E., and Grossman, J. N. 2006. Thermal Metamorphism in Chondrites. In *Meteorites and the Early Solar System II*, edited by D. S. Lauretta and H. Y. McSween Jr., 567–86. Tucson, Arizona: The University of Arizona Press.

Ito, M., Uesugi, M., Naraoka, H., Yabuta, H., Kitajima, F., Mita, H., Takano, Y. et al. 2014. H, C, and N Isotopic Compositions of Hayabusa Category 3 Organic Samples. *Earth, Planets and Space* 66: 102.

Jenniskens, P., Rubin, A. E., Yin, Q.-Z., Sears, D. W. G., Sandford, S. A., Zolensky, M. E., Krot, A. N. et al. 2014. Fall, Recovery, and Characterization of the Novato L6 Chondrite Breccia. *Meteoritics & Planetary Science* 49: 1388–425.

Kitajima, F., Uesugi, M., Karouji, Y., Ishibashi, Y., Yada, T., Naraka, H., Abe, M. et al. 2015. A Micro-Raman and Infrared Study of Several Hayabusa Category 3 (Organic) Particles. *Earth, Planets and Space* 67: 20.

Koga, T., and Naraoka, H. 2017. A New Family of Extraterrestrial Amino Acids in the Murchison Meteorite. *Scientific Reports* 7: 636.

Krot, A. N., Hutcheon, I. D., and Keil, K. 2002. Plagioclase-Rich Chondrules in the Reduced CV Chondrites: Evidence for Complex Formation History and Genetic Links Between Calcium-Aluminum-Rich Inclusions and Ferromagnesian Chondrules. *Meteoritics & Planetary Science* 37: 155–182.

Kvenvolden, K. A., Glavin, D. P., and Bada, J. L. 2000. Extraterrestrial Amino Acids in the Murchison Meteorite: Re-Evaluation After Thirty Years. In *Perspectives in Amino Acid and Protein Geochemistry*, edited by G. A. Goodfriend, M. J. Collins, M. L. Fogel, S. A. Macko, and J. F. Wehmiller, 7–14. New York: Oxford University Press Inc.

Kvenvolden, K., Lawless, J., Pering, K., Peterson, E., Flores, J., Ponnamperuma, C., Kaplan, I. R., and Moore, C. 1970. Evidence for Extraterrestrial Amino-Acids and Hydrocarbons in the Murchison Meteorite. *Nature* 228: 923–6.

Levy, R. L., Grayson, M. A., and Wolf, C. J. 1973. The Organic Analysis of the Murchison Meteorite. *Geochimica et Cosmochimica Acta* 37: 467–83.

Lewis, J. A., Jones, R. H., and Brearley, A. J. 2022. Plagioclase Alteration and Equilibration in Ordinary Chondrites: Metasomatism During Thermal Metamorphism. *Geochimica et Cosmochimica Acta* 316: 201–29.

Lie, Y., Farmer, T. J., and Macquarrie, D. J. 2018. Facile and Rapid Decarboxylation of Glutamic Acid to γ-Aminobutyric Acid via Microwave-Assisted Reaction: Towards Valorisation of Waste Gluten. *Journal of Cleaner Production* 205: 1102–13.

Macke, R. J., Consolmagno, G. J., and Britt, D. T. 2011. Density, Porosity, and Magnetic Susceptibility of Carbonaceous Chondrites. *Meteoritics & Planetary Science* 46: 1842–62.

Martins, Z., Alexander, C. M. O'D., Orzechowska, G. E., Fogel, M. L., and Ehrenfreund, P. 2007. Indigenous

Amino Acids in Primitive CR Meteorites. *Meteoritics & Planetary Science* 42: 2125–36.

Martins, Z., Hofmann, B. A., Gnos, E., Greenwood, R. C., Verchovsky, A., Franchi, I. A., Jull, A. J. T. et al. 2007. Amino Acid Composition, Petrology, Geochemistry, [14]C Terrestrial Age and Oxygen Isotopes of the Shiṣr 033 CR Chondrite. *Meteoritics & Planetary Science* 42: 1581–95.

Messenger, S. 2000. Identification of Molecular-Cloud Material in Interplanetary Dust Particles. *Nature* 404: 968–71.

Nagaoka, H., Takasawa, S., Nakamura, A. M., and Sangen, K. 2014. Degree of Impactor Fragmentation Under Collision with a Regolith Surface—Laboratory Impact Experiments of Rock Projectiles. *Meteoritics & Planetary Science* 49: 69–79.

Naraoka, H., Aoki, D., Fukushima, K., Uesugi, M., Ito, M., Kitajima, F., Mita, H. et al. 2015. ToF-SIMS Analysis of Carbonaceous Particles in the Sample Catcher of the Hayabusa Spacecraft. *Earth, Planets and Space* 67: 67.

Naraoka, H., Mita, H., Hamase, K., Mita, M., Yabuta, H., Saito, K., Fukushima, K. et al. 2012. Preliminary Organic Compound Analysis of Microparticles Returned from Asteroid 25143 Itokawa by the Hayabusa Mission. *Geochemical Journal* 46: 61–72.

Okada, T., Shirai, K., Yamamoto, Y., Arai, T., Ogawa, K., Hosono, K., and Kato, M. 2006. X-Ray Fluorescence Spectrometry of Asteroid Itokawa by Hayabusa. *Science* 312: 1338–41.

Peltzer, E. T., Bada, J. L., Schlesinger, G., and Miller, S. L. 1984. The Chemical Conditions on the Parent Body of the Murchison Meteorite: Some Conclusions Based on Amino, Hydroxy and Dicarboxylic Acids. *Advances in Space Research* 4: 69–74.

Peterson, E., Horz, F., and Chang, S. 1997. Modification of Amino Acids at Shock Pressures of 3.5 to 32 GPa. *Geochimica et Cosmochimica Acta* 61: 3937–50.

Pizzarello, S., and Cronin, J. R. 2000. Non-Racemic Amino Acids in the Murchison and Murray Meteorites. *Geochimica et Cosmochimica Acta* 64: 329–38.

Pizzarello, S., Huang, Y., and Fuller, M. 2004. The Carbon Isotopic Distribution of Murchison Amino Acids. *Geochimica et Cosmochimica Acta* 68: 4963–9.

Pizzarello, S., Zolensky, M., and Turk, K. A. 2003. Nonracemic Isovaline in the Murchison Meteorite: Chiral Distribution and Mineral Association. *Geochimica et Cosmochimica Acta* 67: 1589–95.

Ratcliff Jr., M. A. Medley, E. E., and Simmonds, P. G. 1974. Pyrolysis of Amino Acids. Mechanistic Considerations. *The Journal of Organic Chemistry* 39: 1481–90.

Simkus, D. N., Aponte, J. C., Elsila, J. E., Parker, E. T., Glavin, D. P., and Dworkin, J. P. 2019. Methodologies for Analyzing Soluble Organic Compounds in Extraterrestrial Samples: Amino Acids, Amines, Monocarboxylic Acids, Aldehydes, and Ketones. *Life* 9: 47.

Studier, M. H., Hayatsu, R., and Anders, E. 1968. Origin of Organic Matter in Early Solar System—I. Hydrocarbons. *Geochimica et Cosmochimica Acta* 32: 151–73.

Tenner, T. J., Nakashima, D., Ushikubo, T., Tomioka, N., Kimura, M., Weisberg, M. K., and Kita, N. K. 2019. Extended Chondrule Formation Intervals in Distinct Physicochemical Environments: Evidence from Al-Mg Isotope Systematics of CR Chondrite Chondrules with Unaltered Plagioclase. *Geochimica et Cosmochimica Acta* 260: 133–60.

Uesugi, M., Naraoka, H., Ito, M., Yabuta, H., Kitajima, F., Takano, Y., Mita, H. et al. 2014. Sequential Analysis of Carbonaceous Materials in Hayabusa-Returned Samples for the Determination of Their Origin. *Earth, Planets and Space* 66: 102.

Vallentyne, J. R. 1964. Biogeochemistry of Organic Matter—II Thermal Reaction Kinetics and Transformation Products of Amino Compounds. *Geochimica et Cosmochimica Acta* 28: 157–88.

Van Schmus, W. R., and Wood, J. A. 1967. A Chemical-Petrologic Classification for the Chondritic Meteorites. *Geochimica et Cosmochimica Acta* 31: 747–54.

Weiss, I. M., Muth, C., Drumm, R., and Kirchner, H. O. K. 2018. Thermal Decomposition of the Amino Acids Glycine, Cysteine, Aspartic Acid, Asparagine, Glutamic Acid, Glutamine, Arginine and Histidine. *BMC Biophysics* 11: 2.

Wilkison, S. L., and Robinson, M. S. 2000. Bulk Density of Ordinary Chondrite Meteorites and Implications for Asteroidal Internal Structure. *Meteoritics & Planetary Science* 35: 1203–13.

Yabuta, H., Noguchi, T., Itoh, S., Sakamoto, N., Hashiguchi, M., Abe, K., Tsujimoto, S. et al. 2013. Evidence of Minimum Aqueous Alteration in Rock-Ice Body: Update of Organic Chemistry and Mineralogy of Ultracarbonaceous Antarctic Micrometeorite (Abstract #2335). 44th Lunar and Planetary Science Conference. CD-ROM.

Yabuta, H., Uesugi, M., Naraoka, H., Ito, M., Kilcoyne, A. L. D., Sandford, S. A., Kitajima, F. et al. 2014. X-Ray Absorption Near Edge Structure Spectroscopic Study of Hayabusa Category 3 Carbonaceous Particles. *Earth, Planets and Space* 66: 156.

Yada, T., Fujimura, A., Abe, M., Nakamura, T., Noguchi, T., Okazaki, R., Nagao, K. et al. 2014. Hayabusa-Returned Sample Curation in the Planetary Material Sample Curation Facility of JAXA. *Meteoritics & Planetary Science* 49: 135–53.

Zolensky, M., Herrin, J., Mikouchi, T., Ohsumi, K., Friedrich, J., Steele, A., Rumble, D. et al. 2010. Mineralogy and Petrography of the Almahata Sitta Ureilite. *Meteoritics & Planetary Science* 45: 1618–37.

SUPPORTING INFORMATION

Additional supporting information may be found in the online version of this article.

Table S1. Post-hydrolysis reconstitution volumes and derivatization volumes of the gold foil procedural blank, the Hayabusa particles, and the Murchison sample extracted for amino acid analyses in this study.

Table S2. Detection metrics observed when analyzing a mixed amino acid standard using the analytical technique described in this study.

Table S3. Detection metrics of select non-protein amino acids and glycine in the samples studied here. Mass errors were calculated as described for Table S2.

Table S4. Summary of the D/L ratios and L$_{ee}$ measured for select amino acids in the acid-hydrolyzed

hot water extracts of the CM2 Murchison grain and Hayabusa particles analyzed here.

Fig. S1. Analyses of C_2-C_4 amino acids in analytical reagents prior to their use during sample preparation and analysis indicated only small amounts of Gly and L-Ala were detected in select reagents. The 34- to 46-min LC/ToF-MS chromatograms of m/z 337.0858 for Gly in a mixed amino acid standard (A), ultrapure water intended for use during hot water extraction (B), tdHCl intended for use during acid vapor hydrolysis (C), and a water blank derivatized as described in §1.2 of the supporting information to examine potential uncertainty in amino acid measurements introduced during derivatization (D). The 40- to 55-min LC/ToF-MS chromatograms of m/z 351.1015 for β-Ala and D,L-Ala in a mixed amino acid standard (E), ultrapure water intended for use during hot water extraction (F), tdHCl intended for use during acid vapor hydrolysis (G), and a water blank derivatized as described in §1.2 of the supporting information (H). The 45- to 70-min LC/ToF-MS chromatograms of m/z 365.1171 for C_4 non-protein amino acids in a mixed amino acid standard (I), ultrapure water intended for use during hot water extraction (J), tdHCl intended for use during acid vapor hydrolysis (K), and a water blank derivatized as described in §1.2 of the supporting information (L). The asterisk in trace (E) represents an unidentified peak that did not interfere with target analyte detection. Here, analyte identification follows that described in Table S2. Note: the D-Ala peak in trace (E) is less intense than the corresponding L-Ala peak because of ion suppression experienced due to interference from the coelution of unreacted derivatization agent. Intensities of all reagent mass chromatograms are normalized to those of their corresponding mixed amino acid standard mass chromatograms.

Fig. S2. The Hayabusa particles analyzed here were carbon-rich grains. Prior to amino acid analysis, the Hayabusa particles were analyzed by SEM-EDX, which revealed evidence of organic signatures, such as elemental C, N, and O. SEM-EDX analyses showed elemental compositions for particles #12 (A), #29 (B), #52 (C), #78 (D), and #80 (E), consistent with those described at the JAXA Hayabusa curation facility website (https://curation.isas.jaxa.jp/curation/hayabusa/, accessed 22 February 2022). The spectra shown here are the result of spot analyses. The particles displayed some heterogeneity, but the SEM spectra are representative of the C-rich areas of each grain.

Fig. S3. Schematic of data analysis method employed to determine that strong evidence existed to suggest a portion of the abundance of a detected amino acid was indigenous to the sample. The highlighted route in red exhibits the path used to determine that quantitated sample amino acid abundances were likely to be at least partially indigenous to the sample, as opposed to being solely a product of contamination. If the evaluation criteria of fewer than all five steps of this data analysis method were satisfied by a given amino acid, it was determined that there was insufficient evidence to suggest the amino acid in question was at least partially indigenous to the sample.

Fig. S4. A total of 36 analytes were analyzed for by the analytical technique employed here. The 10- to 100-min region of a fluorescence chromatogram of a mixed amino acid standard. Select amino acids experienced some chromatographic coelution; however, all amino acids that were not fully resolved by chromatography, alone, were fully resolved by a combination of chromatography and accurate mass analysis, except for the enantiomers of α-ABA and Nva. Analyte identifications shown here are consistent with those detailed in Table S2, and are as follows: 1 = D-Asp, 2 = L-Asp, 3 = L-Glu, 4 = D-Glu, 5 = D-Ser, 6 = L-Ser, 7 = D-Ise, 8 = D-Thr, 9 = L-Ise, 10 = L-Thr, 11 = Gly, 12 = β-Ala, 13 = γ-ABA, 14 = D-β-AIB, 15 = L-β-AIB, 16 = D-Ala, 17 = L-Ala, 18 = D-β-ABA, 19 = L-β-ABA, 20 = δ-AVA, 21 = α-AIB, 22 = D,L-α-ABA, 23 = D-Iva, 24 = S-3-APA, 25 = ε-ACA, 26 = L-Iva, 27 = R-3-APA, 28 = L-Val, 29 = D-Val, 30 = D-Nva, 31 = L-Nva, 32 = L-Ile, 33 = 8-AOA, 34 = D-Ile, 35 = D-Leu, 36 = L-Leu.

Fig. S5. The samples and procedural blank were found to be contaminated with ε-ACA; however, contamination did not prevent the detection of other amino acids. The 10- to 100-min fluorescence chromatograms of a mixed amino acid standard (A and E), a blank (B and F), Murchison and #52 (C and G, respectively), and #12,29,80 and #78 (D and H, respectively). The most prominent analyte observed in the blank and samples was the background contaminant, ε-ACA (peak 25). However, the presence of this background contaminant did not prevent the detection of other species that were present at relatively small abundances, such as glycine, β-Ala, and γ-ABA. Analyte identifications shown here are consistent with those detailed in Table S2.

Fig. S6. Accurate mass chromatograms indicated detection of β-Ala in Murchison and #12,29,80. Analysis of β-Ala in a mixed amino acid standard, the procedural blank, Murchison, and #12,29,80, as depicted by their respective 42- to 50-min accurate mass chromatograms for the m/z 351.1015 ± 10 ppm trace. Analyte identifications are consistent with those detailed in Table S2. The β-Ala peak in #12,29,80 was significantly larger than that in the procedural blank, suggesting that while some of the β-Ala signal detected in #12,29,80 is

contributed by the blank, a large portion of the β-Ala signal in #12,29,80 may be indigenous to the sample.

Fig. S7. Accurate mass chromatograms indicated detection of β-AIB and β-ABA in samples analyzed here. Analyses of C_4 non-protein amino acids in a mixed amino acid standard, the procedural blank, Murchison, #12,29,80, #52, and #78, as depicted by their respective 50- to 72-min accurate mass chromatograms for the m/z 365.1171 ± 10 ppm traces. Analyte identifications are consistent with those detailed in Table S2 and are as follows: 13 = γ-ABA,   14 = D-β-AIB,   15 = L-β-AIB, 18 = D-β-ABA, 19 = L-β-ABA, 21 = α-AIB, 22 = D,L-α-ABA. Small quantities of β-AIB were detected in all samples and low abundances of β-ABA were detected primarily in Murchison and #12,29,80. Note: retention times of analytes were shifted for #78 and #52 because these two samples were analyzed on a different day than were the Murchison and #12,29,80 samples.

Fig. S8. Several species were detected above blank levels in the Murchison sample. Blank-uncorrected total abundances of select C_3 to C_5 non-protein amino acids and glycine observed in Murchison compared to corresponding blank levels. Several non-protein amino acids and glycine were observed in Murchison at abundances greater than blank levels. The standard errors reported here were taken from Table 2 of the main manuscript. Note: uncertainties of blank abundances are not shown because replicate blank measurements were not made. However, replicate measurements of other laboratory blanks have indicated that background amino acid abundance estimates are not accompanied by large uncertainty estimates.

Fig. S9. Particle #52 was depleted in amino acids relative to blank levels. Blank-uncorrected total abundances of select C_3 to C_5 non-protein amino acids and glycine observed in #52 compared to corresponding blank levels. The non-protein amino acids, β-ABA and β-AIB were detected at low abundances compared to blank levels, while the other amino acids were depleted relative to blank levels. The standard errors reported here were taken from Table 2 of the main manuscript. Uncertainties of blank relative abundances were not available because of reasons stated in the Fig. S8 legend.

Fig. S10. Particle #78, like #52, was depleted in amino acids relative to blank levels. Blank-uncorrected total abundances of select C_3 to C_5 non-protein amino acids and glycine observed in #78 compared to corresponding blank levels. The nonprotein amino acid, β-AIB was detected at low abundances, but the other species depicted here did not exceed blank levels. The standard errors reported here were taken from Table 2 of the main manuscript. Uncertainties of blank relative abundances were not available because of reasons stated in the Fig. S8 legend.

Fig. S11. Comparisons of amino acid abundances in samples relative to blank levels indicated that select species in Murchison and #12,29,80 were present at abundances distinct from blank levels and thus may be native to their respective samples. Blank-uncorrected abundances, relative to their corresponding blank levels, of select C_3 to C_5 non-protein amino acids and glycine observed in the samples analyzed here. The sample species whose abundances were most strikingly different from blank levels were β- Ala, Ise, and γ-ABA in #12,29,80, and α-AIB and γ-ABA in Murchison. The non-protein amino acids, β-AIB and β-ABA were not included in this comparison because these species were below detection limits in the procedural blank. Note: uncertainty estimates were not provided for amino acid abundances relative to blank levels because of reasons stated in the Fig. S8 legend. Therefore, blank uncertainty estimates were not available to propagate through the appropriate equations.

Fig. S12. The enlarged relative abundance of β-Ala in #12,29,80 supports the hypothesis that a portion of this non-protein amino acid's abundance was likely to be native to the grains analyzed. Blank-uncorrected abundances, relative to glycine, of select non-protein amino acids and alanine observed in the Murchison and #12,29,80 samples studied here. Sample relative abundances were compared to those of the procedural blank to distinguish which sample amino acid relative abundances exceeded those of blank levels beyond sample measurement analytical errors, and were therefore likely to have been contributed by the sample. The standard errors reported here were based on the average values and associated standard errors reported in Table 2 of the main manuscript, and propagated through the appropriate equations. Uncertainties of blank relative abundances were not available because of reasons stated in the Fig. S8 legend.

Fig. S13. The pronounced relative abundance of β-Ala in #12,29,80 suggested this non-protein amino acid's abundance was easily distinguishable from blank levels and thus likely to have been native to the sample. Blank-uncorrected abundances, relative to L-Ala, of select non-protein amino acids and glycine observed in Murchison and #12,29,80. Sample relative abundances were compared to those of the procedural blank to assess the likelihood these sample amino acids may have been contributed by their respective grains. The standard errors reported here were based on the average values and associated standard errors reported in Table 2 of the main manuscript, and propagated through the appropriate equations. Uncertainties of blank relative abundances were not available because of reasons stated in the Fig. S8 legend.

Fig. S14. The abundance, relative to D-Ala, of β-Ala for #12,29,80 remained consistently large, but that of γ-

ABA dropped in contrast to previous relative abundance profiles observed for γ-ABA. Blank-uncorrected abundances, relative to D-Ala, of select non-protein amino acids and glycine observed in Murchison and #12,29,80, compared to blank levels. While the relative abundance profiles of β-Ala for #12,29,80, α-AIB for Murchison, and β-ABA and β-AIB for both Murchison and #12,29,80 remained consistent with previous relative abundance profiles (Fig. S12, S13) and thus suggested these species were attributable to their respective samples, it is noteworthy that the relative abundance profile of γ-ABA for #12,29,80 was strikingly distinct from the previously observed relative abundance profiles of γ-ABA for #12,29,80 (Fig. S12, S13). This contrast indicated that the abundance of γ-ABA for #12,29,80 may likely have been more heavily attributable to the blank than the sample, itself. The standard errors reported here were based on the average values and associated standard errors reported in Table 2 of the main manuscript, and propagated through the appropriate equations. Uncertainties of blank relative abundances were not available because of reasons stated in the Fig. S8 legend.

Data S1. This dataset provides the raw data used to generate the fluorescence chromatograms of Fig. 2 of the main manuscript, which shows the 11- to 63-min regions of the fluorescence chromatograms for a mixed amino acid standard, the procedural blank, Murchison, and #12,29,80.

Data S2. This dataset provides raw data to generate the mass chromatograms shown in Fig. S1 of the supporting information, which illustrates background amino acid abundances present in the analytical reagents used during sample preparation and analysis. In particular, the ultrapure water used for hot water extraction, the tdHCl used for acid vapor hydrolysis, and the derivatization materials were all evaluated for cleanliness prior to exposing samples to these reagents. This test provided a baseline appraisal of amino acid abundance uncertainties contributed by sample preparation and derivatization steps. This test revealed only small amounts of Gly and L-Ala were detected in select reagents used, indicating it was unlikely that large uncertainties in the observed amino acid abundances, namely β-Ala, were introduced by the wet chemical procedures (i.e., extraction, hydrolysis, and derivatization) used here.

Data S3. This dataset provides the raw data used to generate the SEM-EDX spectra shown in Fig. S2 of the supporting information. Fig. S2 of the supporting information shows that the Hayabusa particles analyzed here were carbon-rich and contained such organic signatures as elemental C, N, and O.

Data S4. This dataset provides the raw data used to generate the fluorescence chromatogram shown in Fig. S4 of the supporting information. Fig. S4 of the supporting information shows the 10- to 100-min region of a fluorescence chromatogram of a mixed amino acid standard. Select amino acids experienced some chromatographic coelution; however, all amino acids that were not fully resolved by chromatography, alone, were fully resolved by a combination of chromatography and accurate mass analysis, except for the enantiomers of α-ABA and Nva.

Data S5. This dataset provides the raw data used to generate the fluorescence chromatograms in Fig. S5 of the supporting information, which show the 10- to 100-min chromatograms of a mixed amino acid standard (A and E), a blank (B and F), Murchison and #52 (C and G, respectively), and #12,29,80 and #78 (D and H, respectively). The most prominent analyte observed was the background contaminant, ε-ACA (peak 25). However, the presence of this background contaminant did not prevent the detection of other species present at small abundances (e.g., Gly, β-Ala, and γ-ABA).

Data S6. This dataset provides the raw data used to generate the accurate mass chromatograms shown in Fig. S6 of the supporting information. Fig. S6 of the supporting information shows data from the analysis of β-Ala in a mixed amino acid standard, the procedural blank, Murchison, and #12,29,80, as depicted by their respective 42- to 50-min accurate mass chromatograms for the m/z 351.1015 ± 10 ppm trace. The β-Ala peak in #12,29,80 is significantly larger than that in the procedural blank, suggesting that while some of the β-Ala signal detected in #12,29,80 is contributed by the blank, a large portion of the β-Ala signal in #12,29,80 may be indigenous to the sample.

Data S7. This dataset provides the raw data used to generate the accurate mass chromatograms shown in Fig. S7 of the supporting information. Fig. S7 of the supporting information shows data from the analysis of C_4 non-protein amino acids in a mixed amino acid standard, the procedural blank, Murchison, #12,29,80, #52, and #78, as depicted by their respective 50- to 72-min accurate mass chromatograms for the m/z 365.1171 ± 10 ppm trace. Small quantities of β-AIB were detected in all samples, and low abundances of β-ABA were detected primarily in Murchison and #12,29,80. Note: retention times of analytes were shifted for #78 and #52 because these two samples were analyzed on a different day than were the Murchison and #12,29,80 samples.

Supporting Information for

Non-Protein Amino Acids Identified in Carbon-Rich Hayabusa Particles

Eric T. Parker [1,*], Queenie H.S. Chan [2,3], Daniel P. Glavin [1], Jason P. Dworkin [1]

[1] Astrobiology Analytical Laboratory, Solar System Exploration Division, NASA Goddard Space Flight Center, Greenbelt, MD 20771, U.S.A.;

[2] Department of Earth Sciences, Royal Holloway University of London, Egham, Surrey TW20 0EX, UK;

[3] School of Physical Sciences, The Open University, Walton Hall, Milton Keynes MK7 6AA, UK.

*Corresponding Author: Eric T. Parker
Email: eric.t.parker@nasa.gov
Address: NASA Goddard Space Flight Center, 8800 Greenbelt Road, Mail Code 691, Greenbelt, MD 20771, U.S.A.
Phone Number: 301-614-5107

This document includes:

       Supporting Information text
       Figures S1 to S14
       Tables S1 to S4
       Legends for Datasets S1 to S7

Other supporting information for this manuscript include the following:

       Datasets S1 to S7

Supporting Information Text

1. MATERIALS AND METHODS

1.1. Chemicals and Reagents

Millipore Integral 10 ultrapure water (18.2 MΩ-cm, ≤ 3 ppb total organic carbon) was used for all laboratory work performed in this study. All glassware and other sample handling materials were baked out at 500 °C in air for >10 hours prior to use to remove organic contaminants. The chemical reagents used were purchased from Acros Organics, Sigma-Aldrich, Mann Research Laboratories, EMD Millipore, Fisher Scientific, and Waters Corporation. Individual amino acid crystals used to generate stock analytical standards had purities of ≥96.8 %. All other reagents used here had purities of ≥95 %, unless otherwise stated. Stock solutions of individual amino acids were generated by dissolution of analyte crystals in ultrapure water to produce concentrations of 10^{-3} M and 10^{-1} M. Individual standard solutions were then combined to generate a mixed standard to enable simultaneous analysis of all target analytes.

The specific sample preparation steps that used additional chemical reagents were acid vapor hydrolysis and pre-column derivatization. During acid vapor hydrolysis, 6 M triply distilled hydrochloric acid (tdHCl) was used. During pre-column derivatization, 0.1 M sodium borate, *o*-phthaldialdehyde/*N*-acetyl-L-cysteine (OPA/NAC), and 0.1 M hydrazine hydrate were used, all of which were prepared as described in (Glavin et al., 2021).

Two mobile phases were used during liquid chromatography (LC) analyses: A) 45 mM ammonium formate with 7 % methanol, pH adjusted to 8.9 and B) LC-MS grade methanol. Mobile phase A) was made by first mixing 1.51 mL of formic acid with 780 mL of water, then titrating the solution to pH 9.0 with 1 M aqueous ammonium hydroxide, and finally adding 64 mL of LC-MS methanol. This sequence of steps established a final solution that was 45 mM in ammonium formate, contained 7 % methanol (v:v), and had a final pH of 8.9. The 1 M ammonium hydroxide solution that was used for titration was generated by diluting a 7.6 M stock solution of aqueous ammonium hydroxide (assay = 29.7 %, ammonia basis) with ultrapure water to a final concentration of 1 M.

For time-of-flight mass spectrometry (ToF-MS) analyses, mass calibrations were performed using 0.5 mM sodium formate, and real-time lock mass corrections were executed with 200 µg L^{-1} leucine enkephalin. The preparation of these 2 solutions is detailed elsewhere (Glavin et al., 2021).

The possibility that large uncertainties in amino acid measurements might be derived from the wet chemical procedures (*e.g.,* extraction, hydrolysis, and derivatization) were examined prior to exposing samples to the reagents used during these sample handling steps. Before executing wet chemical procedures, amino acid analyses were performed on: 1) ultrapure water, which examined the potential for uncertainties in amino acid measurements to be introduced during hot water extraction 2) tdHCl, which examined the potential for uncertainties in amino acid measurements to be introduced during acid vapor hydrolysis, and 3) a derivatization blank, which examined the potential for uncertainties in amino acid measurements to be introduced during the derivatization process. Prepared reagents were derivatized as described in §1.2, below and analyzed as detailed in §1.3, below. Fig. S1 shows the background levels of amino acid contamination introduced by each one of these wet chemical procedures for the most abundant amino acid species detected in the samples, C_2-C_4 amino acids. Most common chiral protein amino acids (*e.g.,* Asp, Glu, Ser), are not included in Fig. S1 because their enantiomeric abundances are reported in Table 2 of the Main Manuscript and demonstrate contamination of protein amino acids. Fig. S1 illustrates the results of these analyses. Most common chiral protein amino acids (*e.g.,* Asp, Glu, Ser) are not included in Fig. S1 because their enantiomeric

100 abundances are reported in Table 2 of the Main Manuscript, and demonstrate contamination of
101 protein amino acids.
102   The ultrapure water that was used for hot water extraction was found only to contain
103 trace quantities of glycine (Fig. S1B), while non-protein C_3 and C_4 amino acids were not detected.
104 The tdHCl that was used for acid vapor hydrolysis appeared to be the most likely reagent to
105 introduce uncertainty in downstream amino acid measurements. However, the extent to which
106 this reagent may have contributed uncertainty constituted only small quantities of both glycine
107 (Fig. S1C) and L-alanine (Fig. S1G), while detectable quantities of C_3 and C_4 non-protein amino
108 acids were not observed. Finally, the derivatization blank, which was composed of ultrapure
109 water, 0.1 M sodium borate, OPA/NAC, and 0.1 M hydrazine, was found to possess trace
110 quantities of glycine (Fig. S1D), but not C_3-C_4 non-protein amino acids. Therefore, it is unlikely
111 that large uncertainties in the observed sample amino acid abundances, namely β-Ala, were
112 derived from the wet chemical procedures (*i.e.,* hot water extraction, acid vapor hydrolysis, and
113 derivatization) used here.

1.2. Sample Selection and Preparation

115   Prior to amino acid analysis at NASA Goddard Space Flight Center (GSFC), the
116 carbonaceous material of the Hayabusa samples was analyzed with non-destructive, *in-situ*
117 techniques while hosted in the JAXA dimpled glass slide, including: 1) Fourier-transform infrared
118 micro-spectroscopy (μ-FTIR) at the Spectroscopy and Microscopy in the Infrared using
119 Synchrotron (SMIS) beamline of the synchrotron SOLEIL in France and 2) Raman micro-
120 spectroscopy (μ-Raman) at NASA Johnson Space Center (JSC) and the Open University. The μ-
121 FTIR and μ-Raman results are presented elsewhere (Chan et al., 2019). In short, these particles
122 were found to have IR spectral features (1250 cm^{-1}, 1550 cm^{-1}, and 1650 cm^{-1}) consistent with
123 amides, and Raman spectral features consistent with typical first-order defect and graphite bands
124 (1375 cm^{-1} and 1600 cm^{-1}) indicating the presence of primitive (unheated) organics, making them
125 intriguing candidates for amino acid analysis. Additionally, SEM-EDX analyses suggested the
126 Hayabusa grains were carbon-rich and included signatures of elemental O and N (Fig. S2).

127   Subsequent to μ-FTIR and μ-Raman analyses, the Hayabusa particles were transferred
128 directly from the JAXA dimpled glass slide and pressed into high-purity gold foils, while the
129 Murchison grain was concomitantly pressed into a gold foil square. The sample transferal and
130 pressing processes were conducted in an ISO Class 7 cleanroom, inside a Bassaire laminar flow
131 hood under HEPA-filtered positive pressure (equivalent to ISO Class 4–5) at the Open University.
132 The samples were picked by individual MicroProbes tungsten microneedles (<1 μm tip diameter,
133 previously sterilized by baking in air) using a micromanipulator under an optical microscope
134 objective, and were pressed into the gold foils with individual, sterilized (by baking in air)
135 spectroscopic grade sapphire windows. After pressing onto gold foil, samples were wrapped in
136 baked aluminum foil, sealed in sterile screw-capped glass vials, and mailed to NASA GSFC for
137 amino acid analysis.

138   As noted in the Main Manuscript, particles #12, #29, and #80 were combined prior to
139 analysis. Doing so raised the potential for a limitation of the approach taken here, which is that
140 combining samples prior to analysis prevented the determination of which particles contributed
141 what quantities of which specific amino acids that may be observed from the sample. However, it
142 should be noted that this specific limitation of the approach was accepted after performing a risk-
143 reward analysis in advance of exploring the amino acid chemistry of these grains. It was
144 determined that even though our analytical approach provided state-of-the-art sensitivity for
145 detecting amino acids in small samples, we required particle masses as large as possible such
146 that the particles may be capable of providing a sufficient quantity of amino acid molecules for
147 detection. If the #12, #29, and #80 particles each displayed primitive organic signatures in their
148 Raman spectra, as did particles #52 and #78, we would have considered analyzing each particle
149 (*i.e.,* #12, #29, and #80) individually. However, these three particles did not clearly exhibit
150 primitive organic signatures as did #52 and #78. Given this information and the fact that the

151 objective of the current work was to detect and quantitate the amino acid inventory of Hayabusa
152 particles, it was determined that analyzing these three particles individually would likely be a
153 greater risk to achieving the objective, and that a combined analysis of these three particles was
154 likely to lead to a greater scientific reward by increasing the possibility of observing amino acids.

155 Upon arrival at NASA GSFC, samples were carefully removed from the aluminum foil
156 they were wrapped in and prepared for amino acid extraction inside an ISO 5 HEPA-filtered
157 positive pressure laminar flow hood, located within an ISO ≤8 white room. Samples were then
158 flame-sealed in separate glass ampoules containing 500 µL of water and then underwent hot
159 water extraction for 24 hours at 100 °C. Half of the volume of each hot water extraction
160 supernatant was subjected to acid vapor hydrolysis using 6 M tdHCl for 3 hours at 150 °C to
161 determine total (free + bound) amino acid content. Further details about how samples were
162 handled after hot water extraction and during acid vapor hydrolysis are provided in (Glavin et al.,
163 2006). Following acid vapor hydrolysis, retrieved sample tubes were dried under vacuum to
164 remove HCl. Samples were then rehydrated with 125 µL of water and then dried down under
165 vacuum a second time to ensure full removal of any residual HCl remaining from the acid vapor
166 hydrolysis process. Samples were finally reconstituted with 125 µL of water again, and
167 supernatants were transferred from their respective test tubes, into separate, capped
168 derivatization vials. The sample supernatant volumes (Table S1) that were transferred into
169 derivatization vials were obtained from the respective measured supernatant masses. The entire
170 volume of transferred supernatant for each sample was derivatized as follows: 1) dried down
171 under vacuum, 2) reconstituted in 20 µL of 0.1 M sodium borate, 3) dried down under vacuum, 4)
172 rehydrated with 20 µL of water, 5) derivatized with 5 µL of OPA/NAC (Zhao and Bada, 1995) for
173 15 minutes at room temperature, and 6) quenched with 75 µL of 0.1 M hydrazine hydrate. The
174 derivatized samples were then immediately analyzed by LC-FD/ToF-MS.

175 ### *1.3. Amino Acid Analysis*

176 Amino acids were analyzed by LC-FD/ToF-MS using a Waters Acquity H-Class ultrahigh
177 performance liquid chromatograph, coupled to a Waters Acquity fluorescence detector, and a
178 Waters Xevo G2-XS time-of-flight mass spectrometer. Compound identifications were determined
179 by chromatographic retention time, optical fluorescence, and accurate mass measurements,
180 based on comparison to a mixed amino acid standard.

181 Chromatographic separation was achieved using the following 3 columns in series: 1) 2.1
182 x 150 mm, 1.7 µm particle size Waters Acquity CSH Phenyl-Hexyl, 2) 2.1 x 100 mm, 1.7 µm
183 particle size Waters Acquity CSH C18, and 3) 2.1 x 150 mm, 1.7 µm particle size Waters Acquity
184 CSH Phenyl-Hexyl. Amino acids were eluted using the following gradient: 0 – 60 min, 100 – 67 %
185 eluent A, 60 – 70 min, isocratic at 67 % eluent A, 70 – 75 min, 67 – 55 % eluent A, 75 – 80 min,
186 isocratic at 55 % eluent A, 80 – 100 min, 55 - 17 % eluent A, 100 – 100.1 min, 17 – 0 % eluent A,
187 100.1 – 105 min, isocratic at 0 % eluent A, 105 – 105.1 min, 0 – 100 % eluent A, 105.1 – 120 min,
188 isocratic at 100 % eluent A. The eluent flow rate was 0.11 mL min^{-1} for the entirety of the run and
189 columns were heated at 34 °C. The autosampler was kept at a constant temperature of 5 °C and
190 the injection volume was 10 µL. The fluorescence detector (FD) was operated with an excitation
191 wavelength of 340 nm and an emission wavelength of 450 nm.

192 The ToF-MS system utilized a dual ESI source setup, both of which were operated in
193 positive ion mode. The primary ESI source was utilized according to the following parameters:
194 source temperature: 120 °C, capillary voltage: 1.2 kV, sampling cone voltage: 40 V, cone gas (N_2)
195 flow: 50 L hr^{-1}, desolvation gas (N_2) temperature: 500 °C, and desolvation gas flow: 300 L hr^{-1}.
196 The primary ESI source was calibrated daily over the 50 – 1200 *m/z* range. The purpose of using
197 the secondary ESI source was to account for small deviations in the *m/z* scale that may occur
198 over a 24-hour period, following the completion of daily calibrations. The secondary ESI source
199 achieved this objective by providing an independent standard signal of leucine enkephalin at *m/z*
200 556.2771. The secondary ESI source was operated with identical parameters to those of the

201   primary ESI source, except the secondary ESI source used a capillary voltage of 2.8 kV and a
202   reference cone voltage of 30 V. The ToF-MS analyzer was operated in V-optics mode, which
203   used a reflectron to achieve a full width at half maximum resolution of 22,000 based on the
204   independent mas signal of leucine enkephalin. The detector voltage setting used was 2850 V,
205   and data were collected over a mass range of 50 – 900 *m/z*. A mass tolerance of 10 parts per
206   million (ppm) was implemented for the purpose of accurate mass identification of target analytes
207   by ToF-MS.

208   *1.3.1. Absolute Quantitation*

209   Absolute quantitation was performed in four steps. The first step was to determine gold
210   foil procedural blank amino acid abundances. This was achieved by comparing gold foil
211   procedural blank analyte peak areas to the peak areas and concentrations of the respective
212   standard analytes, while accounting for the volume of ultrapure water the procedural blank was
213   reconstituted in after acid vapor hydrolysis (Table S1), the mass (2.16 mg, Table 1 of the Main
214   Manuscript) of the gold foil used for the procedural blank as a proxy for its surface area, and the
215   different derivatization volumes used for the standard (10 μL) and the procedural blank (110.102
216   μL, Table S1):

$$B_A \; = \; \left[\frac{C_R \; \times \; D_R \; \times \; A_B \; \times \; V_B \; \times \; 10^9}{A_R \; \times \; D_B \; \times \; M_B^F} \right] \tag{S1}$$

217   In equation (S1), B_A is the procedural blank amino acid abundance, in units of nmol g^{-1},
218   for a given analyte, C_R is the concentration, in units of mol L^{-1}, of the associated reference (*i.e.,*
219   standard) analyte, D_R is the volume, in units of liters, of the reference (*i.e.,* standard) mixture that
220   was derivatized, A_B is the peak area, with arbitrary units, of the respective analyte in the
221   procedural blank, V_B is the volume, in units of liters, that the procedural blank was reconstituted in
222   after acid vapor hydrolysis, 10^9 is the conversion factor from units of mol to nmol, A_R is the peak
223   area, with arbitrary units, of the reference analyte, D_B is the volume, in units of liters, of the
224   procedural blank that was derivatized, and M_B^F is the mass, in units of grams, of the gold foil
225   square that was used for the procedural blank. Thus, equation (S1) calculated the background
226   amino acid abundances for the procedural blank, which was comprised of a gold foil square with
227   a surface area that corresponded to a mass of 2.16 mg and a derivatized volume of 110.102 μL.

228   Since the procedural blank was prepared using a gold foil with a different surface area
229   and mass by which to potentially serve as a source of contamination (see Table 1 of the Main
230   Manuscript for details) and a different derivatized volume (see Table S1 for details), compared to
231   those for each sample, it is likely that the gold foil procedural blank amino acid abundances
232   calculated using equation (S1) did not accurately represent the abundances of background amino
233   acids in each of the samples, assuming an equal distribution of these species across the surface
234   areas of the gold foil squares used and throughout the sample preparation and derivatization
235   reagents used. Consequently, the second step of the absolute quantitation process accounted for
236   such disparities by calculating extrapolated background amino acid abundances for each sample.
237   The extrapolated background amino acid abundances for each sample were based on the amino
238   acid abundances observed for the gold foil procedural blank, while controlling for differences
239   between the procedural blank and samples with respect to derivatization volumes used and gold
240   foil surface areas used, with gold foil masses serving as a proxy for this variable:

$$B_A' \; = \; \left[\frac{C_R \; \times \; D_R \; \times \; A_B \; \times \; V_S \; \times \; 10^9}{A_R \; \times \; D_S \; \times \; M_S^F} \right] \; = \; B_A \; \times \; \left[\frac{D_B \; \times \; M_B^F}{D_S \; \times \; M_S^F} \right] \tag{S2}$$

241   In equation (S2), B_A' is the extrapolated background amino acid abundance, in units of
242   nmol g^{-1}, of the analyte in question for a given sample, V_S is the volume of ultrapure water the

5

243   sample was reconstituted in after acid vapor hydrolysis (Table S1), D_S is the volume, in units of
244   liters, of the sample that was derivatized, and M_S^F is the mass, in units of grams, of the gold foil
245   that was used for the respective sample. Therefore, equation (S2) was used to calculate the
246   extrapolated background amino acid abundances for a given sample, while taking into account
247   the differences in the surface areas (using masses as a proxy) of the gold foil squares used and
248   associated derivatization volumes of each sample compared to the gold foil procedural blank.

249   The third step of the absolute quantitation process was to calculate blank-uncorrected
250   amino acid abundances for each sample by comparing the sample analyte peak areas to the
251   peak areas and concentrations of the respective standard analytes, while accounting for the
252   volume of ultrapure water the sample was reconstituted in after acid vapor hydrolysis (Table S1),
253   the combined mass of the gold foil square used for the sample in question and the estimated
254   mass of the pressed sample (see Table 1 of the Main Manuscript for details) as a proxy for the
255   total combined surface area of the gold foil and the pressed sample, and the different
256   derivatization volumes used for the standard (10 μL) and the sample of interest (see Table S1 for
257   details):

$$S_U = \left[\frac{C_R \ \times \ D_R \ \times \ A_S \ \times \ V_S \ \times \ 10^9}{A_R \ \times \ D_S \ \times \ M_S} \right] \tag{S3}$$

258   In equation (S3), S_U is the blank-uncorrected amino acid abundance, in units of nmol g^{-1},
259   for a given analyte for the sample of interest, A_S is the peak area, with arbitrary units, of the
260   respective analyte for the sample, and M_S is the combined mass, in units of grams, of the relevant
261   gold foil square and the pressed sample of interest. Therefore, equation (S3) provided an amino
262   acid abundance that was equivalent to the sum of the extrapolated background amino acid
263   abundances for each sample and the amino acid abundances associated with the estimated
264   mass of the pressed sample.

265   Finally, the fourth step of the absolute quantitation process was to subtract the
266   extrapolated background amino acid abundances (equation S2) from the blank-uncorrected
267   amino acid abundances of the respective sample (equation S3) to determine the blank-corrected
268   amino acid abundances for a given sample:

$$S_A = S_U \ - \ B_A' \tag{S4}$$

269   In equation (S4), S_A is the blank-corrected amino acid abundance, in units of nmol g^{-1}, for
270   a given analyte in a given sample. Thus, equation (S4) provided the final, blank-corrected
271   abundances of amino acids reported in Table 2 of the Main Manuscript.

272   *1.3.2. Determination of Amino Acid Indigeneity to Sample*

273   Due to the low amino acid abundances in the extracts of grains analyzed here, combined
274   with the presence of trace quantities of contamination observed, it was imperative to employ a
275   method by which to distinguish amino acid detections that were likely to be indigenous to the
276   sample, despite the presence of contamination. The likelihood that a detected amino acid was
277   indigenous to the sample in question, as opposed to being solely the product of contamination,
278   was determined using a multi-step data analysis method: 1) comparison of blank-uncorrected
279   sample amino acid abundances, relative to corresponding blank levels, 2) comparison of blank-
280   uncorrected sample amino acid abundances, relative to glycine (a common terrestrial
281   contaminant), to corresponding blank levels, 3) comparison of blank-uncorrected sample amino
282   acid abundances, relative to an additional common terrestrial contaminant (D+L-Ala), to
283   corresponding blank levels, and 4) and 5) comparison of blank-uncorrected sample amino acid
284   abundances, relative to the L- and D-enantiomers, respectively, of alanine, to corresponding

285 blank levels (Fig. S3). Therefore, this data analysis method was used to evaluate the strength of
286 the evidence to suggest amino acid provenance with respect to the sample.

287   The implications of the results of each of the steps depicted in Fig. S3 are described
288 here. Step 1) was used to determine if the blank-uncorrected abundance of a given sample amino
289 acid was substantially ($\gtrsim$2 times) larger than the corresponding blank levels. If the amino acid in
290 question satisfied the evaluation criteria of Step 1), the evaluation proceeded to Step 2). Step 2)
291 was used to assess if the blank-uncorrected abundance, relative to a common terrestrial
292 contaminant like glycine, of a given sample amino acid exceeded (*i.e.,* beyond sample
293 measurement analytical errors) that of the corresponding blank levels. If the amino acid in
294 question satisfied the evaluation criteria of Step 2), the evaluation proceeded to Step 3). Since
295 comparisons relative to glycine are a somewhat porous filter given the difficulty of assessing
296 glycine contamination in such small samples, comparisons relative to glycine were performed to
297 assess relative abundance profiles of sample amino acids as a rudimentary approximation.
298 However, it was necessary to more rigorously evaluate correlations between sample amino acid
299 relative abundances and those of common terrestrial contaminants. For this purpose, Step 3)
300 performed the same type of evaluations as Step 2), but with respect to D+L-Ala, as opposed to
301 glycine. If the outcome of Step 3) was consistent with that of Step 2) (*i.e.,* blank-uncorrected
302 sample relative abundances exceeded the corresponding blank levels beyond the margins of
303 analytical errors for the sample measurement), the evaluation proceeded to Step 4). Step 4)
304 performed the same type of evaluations as Steps 2) and 3), but with respect to L-Ala, which is the
305 alanine enantiomer that is more commonly associated with terrestrial contamination. If the
306 outcome of Step 4) was consistent with that of Step 3), the evaluation proceeded to Step 5). Step
307 5) was identical to step 4), except L-Ala in Step 4) was replaced with D-Ala in Step 5). Since the
308 D-enantiomer of alanine is less commonly associated with terrestrial contamination than the L-
309 enantiomer of alanine, comparisons of relative abundances to D-Ala can help discern between
310 sample amino acid abundances that were likely to be largely due to terrestrial contamination and
311 those that were not. An outcome from Step 5) consistent with that of Steps 3) and 4), indicated
312 the abundance profile of the sample amino acid in question was not likely to be due solely to
313 terrestrial contamination. It must be underscored that only if the sample amino acid in question
314 satisfied the evaluation criteria of all five aforementioned steps, was it determined that strong
315 evidence existed to suggest the detected amino acid was sufficiently dissimilar from blank levels
316 to support the assertion that a portion of that amino acid's abundance was indigenous to the
317 respective sample. It should also be noted that due to the nature of this multi-step evaluation
318 approach, with respect to its incorporation of protein amino acid data as the normalizing factors,
319 this data analysis method is only considered effective for evaluating non-protein amino acid
320 indigeneity to samples.
321
322 **2. RESULTS AND DISCUSSION**

323 ***2.1. Analytical Performance***

324   The chromatography implemented in this study was optimized to resolve 22 target amino
325 acids, including the enantiomers of 15 chiral amino acids (Fig. S4). The amino acids of interest in
326 this study are detailed in Table S2. At or near baseline resolution was achieved for the most
327 analytes when analyzed by fluorescence (Fig. S4). Notable exceptions include the coelutions of
328 D-Thr and L-Ise, L-β-ABA and δ-AVA, D-α-ABA and L-α-ABA, ϵ-ACA and L-Iva, and D-Nva and
329 L-Nva. The enantiomers of α-ABA could not be resolved by the chromatography employed, while
330 the enantiomers of Nva were partially resolved. The remaining examples of coelution were fully
331 resolved when analyzed by accurate mass. Therefore, the enantiomers of α-ABA and Nva were
332 the only analytes for which at or near baseline resolution was not achieved by one of the
333 detectors used here. The efficacy of the optimized LC-FD/ToF-MS technique used in this work is
334 displayed in Table S2, which demonstrates the consistencies of the retention times observed
335 between the FD and ToF-MS detectors, and the associated measured mass accuracies of the
336 target analytes in a mixed amino acid standard.

2.2. Amino Acid Detections

An immediate observation that was made upon analysis was the presence of a relatively large abundance of the C_6 amino acid, ε-ACA, in the procedural blank and the samples (Fig. S5). The amino acid ε-ACA is the main product of nylon 6 hydrolysis, and nylon contaminants are challenging to eliminate as they are common in cleanrooms and prevalent in materials found in laboratories, such as casters, ties, wipes, and bags (Dworkin et al., 2018). A laboratory analytical blank composed of ultrapure water was processed in parallel with the gold foil procedural blank and samples, and was also contaminated with ε-ACA, although at an abundance $\approx$7.5 times lower than that observed for the procedural blank. The presence of ε-ACA in the laboratory analytical blank suggests this contaminant likely originated from the laboratory. In addition to ε-ACA, there were trace levels of other amino acids observed in the blank, including protein amino acids, which is consistent with contamination. Despite the presence of contamination, it is important to note that background contaminants did not prevent the observation of target analytes present in samples at abundances greater than blank levels.

Amino acid detections of most interest in this study were not those that were likely to be contamination, such as chiral protein amino acids with large L-enantiomeric excesses (L_{ee}) in samples (*e.g.,* L-Ala, L-Asp, L-Thr, L-Glu, L-Val, L-Leu, or L-Ile). Instead, the non-protein C_3 *n-ω*-amino acid, β-Ala, and the non-protein C_4 amino acids, γ-ABA, β-AIB, β-ABA, and α-AIB were examples of the types of amino acids that were of chief interest during analysis. Fig. S6 and S7 show examples of how the possible detections of these amino acids in samples were evaluated in comparison to the procedural blank and a mixed amino acid standard. For example, Fig. S6 illustrates that while β-Ala was slightly more prominent in Murchison than the blank, this amino acid was observed to be significantly more elevated in #12,29,80. Additionally, Fig. S7 demonstrates that γ-ABA and α-AIB were detected in select samples at levels greater than those observed for the procedural bank, but notably small quantities of species like β-AIB and β-ABA were often detected in samples, but not the procedural blank. Lastly, although a signal for α-AIB was observed for #52 and #78, α-AIB abundances for these grains did not exceed blank levels and thus were not reported in Table 2 of the Main Manuscript.

The most intriguing examples of amino acid detections and tentative identifications are select C_3 to C_5 non-protein amino acids and glycine reported in Table S3, which provides detection metrics observed for these species in each sample. The tentative identifications of glycine, isoserine, and δ-AVA for Murchison and #12,29,80 are categorized as such because although these compounds were preliminarily detected by fluorescence, their accurate masses were measured outside the 10-ppm mass tolerance window due to interferences in the mass spectra with unidentified analytes that possessed similar retention times and accurate masses as the target analytes. However, β-Ala, γ-ABA, β-AIB, β-ABA, and α-AIB for Murchison and #12,29,80 all exhibited close detection metric agreement with those of a mixed amino acid standard, providing confidence in the detections of these analytes. In contrast, β-AIB was the lone amino acid most confidently detected for #52 and #78, due in part to the high degree of fidelity in this analyte's observed detection metrics between the samples and a mixed amino acid standard. Lastly, it should be noted that the presence of trace-level peaks associated with the *m/z* values of C_7-C_9 amino acids was observed in the Murchison and #12,29,80 accurate mass chromatograms. The identities of these trace-level peaks were not possible to confidently determine in the current exploration and would require a more detailed study to further evaluate.

2.3. Amino Acid Abundances

Quantitative analyses of amino acids are important to determine if their presence is likely to be indigenous to the samples or terrestrial contamination. In this context, the total blank-uncorrected abundances of the aforementioned C_3 to C_5 non-protein amino acids and glycine were compared to their respective blank levels for Murchison (Fig. S8), #52 (Fig. S9), and #78 (Fig. S10). For Murchison, glycine, β-Ala, α-AIB, β-ABA, β-AIB, and γ-ABA appear most notably

387 larger in the sample than blank levels, and therefore are candidates to be at least partially
388 indigenous to the CM2 Murchison grain analyzed. Conversely, most species are notably less
389 abundant in #52 and #78 compared to their respective blank levels, except for β-ABA and β-AIB.
390 Given that these species were not detected in the procedural blank, β-ABA and β-AIB are
391 indigenous to their respective grains (Fig. S8-S10).

392 Aside from β-ABA and β-AIB, which were readily indigenous to their respective samples
393 for reasons noted above, the other amino acids that constitute the C_3 to C_5 non-protein amino
394 acids of interest required further examination to determine their sample indigeneity, as trace
395 levels of these species were observed in the gold foil procedural blank. Therefore, a detailed
396 accounting of the implementation of the previously mentioned multi-step data analysis method to
397 determine amino acid indigeneity to samples in the face of trace contamination, is provided here.
398 Application of Step 1) (Fig. S3) results in the comparison of blank-uncorrected abundances,
399 relative to their corresponding blank levels, of the aforementioned C_3 to C_5 non-protein amino
400 acids and glycine for a given sample (Fig. S11). Notable absences from Fig. S11 are β-AIB and
401 β-ABA as these compounds were not detected in the procedural blank and are therefore strongly
402 considered to be native to their respective samples. When evaluating sample amino acid
403 abundances, relative to blank levels, relative abundances ≲1 indicate amino acid species present
404 in samples at abundances similar to or less than blank levels and thus are likely to be indigenous
405 to the blank. This is consistent with the approach of Naraoka et al. (Naraoka et al., 2012), which
406 detected D,L-Ala and Gly in two Itokawa grains at abundances similar to blank levels
407 (abundances of 0.5 – 1.6, relative to blank = 1), and reported these detections as mostly
408 contaminants. Based on the Naraoka et al. (Naraoka et al., 2012) approach, a screening
409 procedure was used here such that a sample amino acid with an abundance, relative to blank
410 levels, of ≳2, were considered substantially larger than that observed in the blank, such that a
411 portion of the sample amino acid abundance may likely be indigenous to the grains themselves.
412 Taking this into consideration, it can be seen than none of the species of interest have a relative
413 abundance of ≳2 for #52 and #78 (Fig. S11). However, for Murchison, a relative abundance >3
414 was observed for α-AIB and ≈2 for γ-ABA, and for #12,29,80, β-Ala was ≈4.5 times more
415 abundant than blank levels, while isoserine, and γ-ABA had relative abundances ≳2 (Fig. S11).
416 Aside from isoserine, which was only tentatively identified in #12,29,80 (Table S3), the following
417 species are considered to have satisfied the evaluation criteria of Step 1) (Fig. S3): α-AIB for
418 Murchison, β-Ala for #12,29,80, γ-ABA for Murchison and #12,29,80, β-ABA for all samples
419 except #78, and β-AIB for all samples.

420 The abundance profiles of the sample C_3 to C_5 non-protein amino acids were further
421 evaluated by comparing their abundances, relative to glycine (Step 2, Fig. S3), D+L-Ala (Step 3),
422 Fig. S3), L-Ala (Step 4), Fig. S3), and D-Ala (Step 5), Fig. S3), to blank levels, as shown in Fig.
423 S12, Fig. 4 of the Main Manuscript, Fig. S13, and Fig. S14, respectively. When comparing amino
424 acid abundances relative to glycine, β-Ala in #12,29,80, α-AIB in Murchison, and β-AIB, β-ABA,
425 and γ-ABA in both Murchison and #12,29,80 have relative abundances that exceed blank levels
426 beyond the sample measurement analytical errors (Fig. S12). This finding suggests that α-AIB for
427 Murchison, β-Ala for #12,29,80, γ-ABA for Murchison and #12,29,80, β-ABA for all samples
428 except #78, and β-AIB for all samples have satisfied the evaluation criteria of Step 2) (Fig. S3).
429 Worthy of note, the ratio of the β-Ala abundance, relative to glycine, of #12,29,80 compared to
430 blank levels is the largest observed ratio, at 2.4. When comparing amino acid abundances
431 relative to D+L-Ala, it can be seen that the comparative results (Fig. 4 of the Main Manuscript) of
432 the aforementioned species of interest are consistent with those observed for the amino acid
433 abundances relative to glycine. This result suggests that α-AIB for Murchison, β-Ala for
434 #12,29,80, γ-ABA for Murchison and #12,29,80, β-ABA for all samples except #78, and β-AIB for
435 all samples have satisfied the evaluation criteria of Step 3) (Fig. S3). Similar to amino acid
436 abundances relative to glycine, the ratio of β-Ala abundance, relative to D+L-Ala, for #12,29,80
437 compared to blank levels is consistently the largest ratio observed, at 2.5. In comparing amino
438 acid abundances, relative to L-Ala, it can be seen these results (Fig. S13) are consistent with

439 those observed for the abundances relative to D+L-Ala. This finding suggests that α-AIB for
440 Murchison, β-Ala for #12,29,80, γ-ABA for Murchison and #12,29,80, β-ABA for all samples
441 except #78, and β-AIB for all samples have satisfied the evaluation criteria of Step 4) (Fig. S3).
442 The results of comparing C_3 to C_5 non-protein amino acid abundances relative to D-Ala (Fig. S14)
443 are all consistent with those observed for the abundances relative to glycine, D+L-Ala, and L-Ala,
444 except for γ-ABA in #12,29,80. The abundance of γ-ABA, relative to D-Ala, for #12,29,80 was
445 below blank levels, whereas the abundances of γ-ABA, relative to glycine, D+L-Ala, and L-Ala for
446 #12,29,80 were all greater than blank levels beyond sample measurement analytical errors. Since
447 D-Ala is less commonly associated with terrestrial contamination than glycine or L-Ala, the
448 observed discrepancy of γ-ABA relative abundance profiles for #12,29,80 suggests that the
449 elevated abundances of γ-ABA, relative to glycine, D+L-Ala, and L-Ala, for #12,29,80 compared
450 to blank levels, may be more heavily influenced by contamination than the other C_3 to C_5 non-
451 protein amino acids. Therefore, γ-ABA did not satisfy the evaluation criteria of Step 5) (Fig. S3).
452 As a result, of the C_3 to C_5 non-protein amino acids of interest, the comparative data brought
453 about by the sequence of evaluation criteria implemented here indicates that a portion of the
454 abundances of the following amino acids are considered likely to be indigenous to the sample: β-
455 Ala in #12,29,80, α-AIB and γ-ABA in Murchison, β-ABA in all samples except #78, and β-AIB in
456 all samples analyzed here.
457
458 ***2.4. Enantiomeric Analyses***

459   A primary benefit of the OPA/NAC derivatization approach used here was that it
460 facilitated the quantitative analysis of the enantiomers of all chiral amino acids that were detected
461 in samples. In turn, this can yield important information regarding the possible extraterrestrial
462 nature of target amino acids. Chiral protein amino acids with large L_{ee} are often considered to be
463 of terrestrial origin, whereas protein and non-protein amino acids with D/L ratios ≈1 are indicative
464 of abiotic synthetic pathways. Additionally, non-protein amino acids that are rare in biology and
465 are accompanied by slight L_{ee} have previously been shown to be a product of extraterrestrial
466 synthesis, which holds important implications for the origin of homochirality (Cronin and
467 Pizzarello, 1997; Elsila et al., 2016; Engel and Macko, 1997; Glavin and Dworkin, 2009;
468 Pizzarello and Cronin, 2000; Pizzarello et al., 2003).

469   In the current work, all chiral protein amino acids detected were present mostly as the L-
470 enantiomer at trace abundances (Table 2 of the Main Manuscript), which is indicative of terrestrial
471 contamination. However, the chiral non-protein amino acids detected in this work showed more
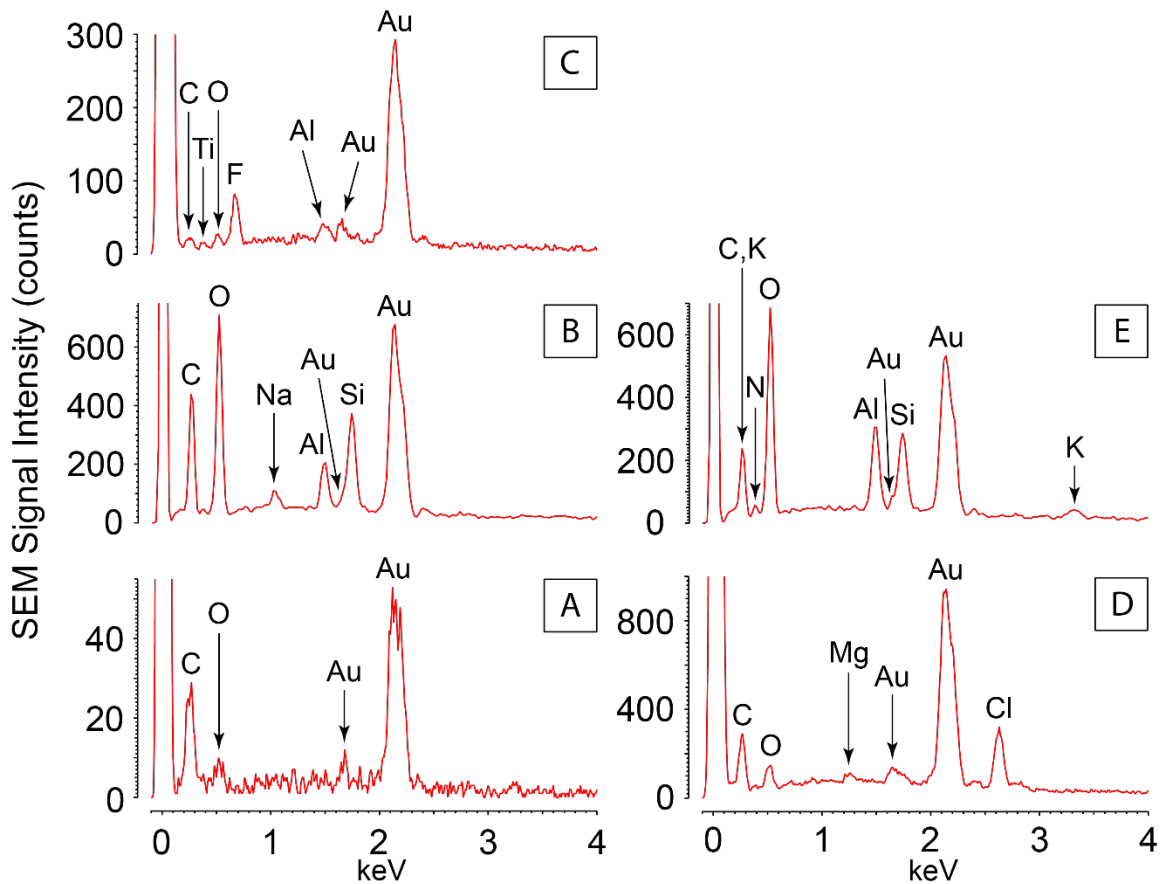472 variability in their D/L ratios. Select examples of such variabilities are detailed in Table S4**.**

SUPPORTING INFORMATION REFERENCES

473

474 Chan, Q.H.S., Zolensky, M.E., Brunetto, R., Parker, E.T., Dworkin, J.P., Sandt, C., Wright, I.P.,
475 Franchi, I.A., 2019. Coordinated organic analyses of Hayabusa category 3 carbonaceous
476 particles, 82nd Annual Meeting of The Meteoritical Society, Sapporo, Japan, p. 6223.

477 Cronin, J.R., Pizzarello, S., 1997. Enantiomeric excesses in meteoritic amino acids. Science 275,
478 951-955.

479 Dworkin, J.P., Adelman, L.A., Ajluni, T., Andronikov, A.V., Aponte, J.C., Bartels, A.E., Beshore,
480 E., Bierhaus, E.B., Brucato, J.R., Bryan, B.H., Burton, A.S., Callahan, M.P., Castro-Wallace, S.L.,
481 Clark, B.C.C., S.J., Connolly Jr., H.C., Cutlip, W.E., Daly, S.M., Elliott, V.E., Elsila, J.E., Enos,
482 H.L., Everett, D.F., Franchi, I.A., Glavin, D.P., Graham, H.V., Hendershot, J.E., Harris, J.W., Hill,
483 S.L., Hilderand, A.R., Jayne, G.O., Jenkens Jr., R.W., Johnson, K.S., Kirsch, J.S., Lauretta, D.S.,
484 Lewis, A.S., Loiacono, J.J., Lorentson, C.C., Marshall, J.R., Martin, M.G., Matthias, L.L., McLain,
485 H.L., Messenger, S.R., Mink, R.G., Moore, J.L., Nakamura-Messenger, K., Nuth III, J.A., Owens,
486 C.V., Parish, C.L., Perkins, B.D., Pryzby, M.S., Reigle, C.A., Righter, K., Rizk, B., Russell, J.F.,
487 Sandford, S.A., Schepis, J.P., Songer, J., Sovinski, M.F., Stahl, S.E., Thomas-Keprta, K.,
488 Vellinga, J.M., Walker, M.S., 2018. OSIRIS-REx Contamination Control Strategy and
489 Implementation. Space Sci. Rev. 214.

490 Elsila, J.E., Aponte, J.C., Blackmond, D.G., Burton, A.S., Dworkin, J.P., Glavin, D.P., 2016.
491 Meteoritic Amino Acids: Diversity in Compositions Reflects Parent Body Histories. ACS Cent. Sci.
492 2, 370-379.

493 Engel, M., Macko, S., 1997. Isotopic evidence for extraterrestrial non-racemic amino acids in the
494 Murchison meteorite. Nature 389, 265-268.

495 Glavin, D.P., Dworkin, J.P., 2009. Enrichment of the amino acid L-isovaline by aqueous alteration
496 on CI and CM meteorite parent bodies. Proc. Natl. Acad. Sci. U. S. A. 106, 5487-5492.

497 Glavin, D.P., Dworkin, J.P., Aubrey, A., Botta, O., Doty, J.H., Martins, Z., Bada, J.L., 2006. Amino
498 acid analyses of Antarctic CM2 meteorites using liquid chromatography-time of flight-mass
499 spectrometry. Meteorit. Planet. Sci. 41, 889-902.

500 Glavin, D.P., Elsila, J.E., McLain, H., Aponte, J.C., Parker, E.T., Dworkin, J.P., Hill, D.H.,
501 Connolly Jr., H.C., Lauretta, D.S., 2021. Extraterrestrial amino acids and L-enantiomeric
502 excesses in the CM2 carbonaceous chondrites Aguas Zarcas and Murchison. Meteorit. Planet.
503 Sci. 56, 148-173.

504 Naraoka, H., Mita, H., Hamase, K., Mita, M., Yabuta, H., Saito, K., Fukushima, K., Kitajima, F.,
505 Sandford, S.A., Nakamura, T., Noguchi, T., Okazaki, R., Nagao, K., Ebihara, M., Yurimoto, H.,
506 Tsuchiyama, A., Abe, M., Shirai, K., Ueno, M., Yada, T., Ishibashi, Y., Okada, T., Fujimura, A.,
507 Mukai, T., Yoshikawa, M., Kawaguchi, J., 2012. Preliminary organic compound analysis of
508 microparticles returned from Asteroid 25143 Itokawa by the Hayabusa mission. Geochem. J. 46,
509 61-72.

510 Pizzarello, S., Cronin, J.R., 2000. Non-racemic amino acids in the Murray and Murchison
511 meteorites. Geochim. Cosmochim. Acta 64, 329-338.

512 Pizzarello, S., Zolensky, M., Turk, K.A., 2003. Nonracemic isovaline in the Murchison meteorite:
513 Chiral distribution and mineral association. Geochim. Cosmochim. Acta 67, 1589-1595.

514 Zhao, M., Bada, J.L., 1995. Determination of α-dialkylamino acids and their enantiomers in
515 geological samples by high-performance liquid chromatography after derivatization with a chiral
516 adduct of *o*-phthaldialdehyde. J. Chromatogr. A 690, 55-63.
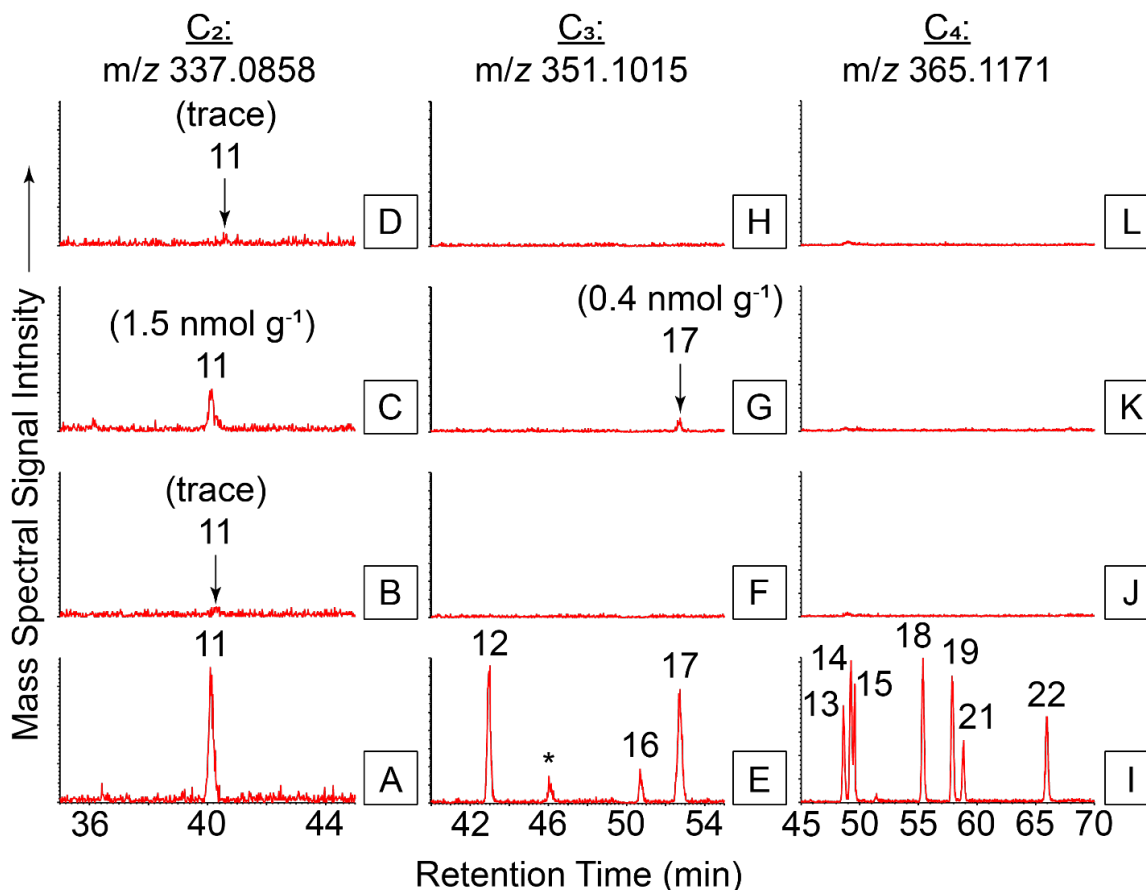
517 **FIGURES AND TABLES**

519 ***Fig. S1. Analyses of C₂-C₄ amino acids in analytical reagents prior to their use during***
520 ***sample preparation and analysis indicate only small amounts of Gly and L-Ala were***
521 ***detected in select reagents.*** The 34 – 46-minute LC/ToF-MS chromatograms of m/z 337.0858
522 for Gly in a mixed amino acid standard (A), ultrapure water intended for use during hot water
523 extraction (B), tdHCl intended for use during acid vapor hydrolysis (C), and a water blank
524 derivatized as described in §1.2 of the Supporting Information to examine potential uncertainty in
525 amino acid measurements introduced during derivatization (D). The 40 – 55-minute LC/ToF-MS
526 chromatograms of m/z 351.1015 for β-Ala and D,L-Ala in a mixed amino acid standard (E),
527 ultrapure water intended for use during hot water extraction (F), tdHCl intended for use during
528 acid vapor hydrolysis (G), and a water blank derivatized as described in §1.2 of the Supporting
529 Information (H). The 45 – 70-minute LC/ToF-MS chromatograms of m/z 365.1171 for C₄ non-
530 protein amino acids in a mixed amino acid standard (I), ultrapure water intended for use during
531 hot water extraction (J), tdHCl intended for use during acid vapor hydrolysis (K), and a water
532 blank derivatized as described in §1.2 of the Supporting Information (L). The asterisk in trace (E)
533 represents an unidentified peak that did not interfere with target analyte detection. Here, analyte
534 identification follows that described in Table S2. Note: the D-Ala peak in trace (E) is less intense
535 than the corresponding L-Ala peak because of ion suppression experienced due to interference
536 from the coelution of unreacted derivatization agent. Intensies of all reagent mass
537 chromatograms are normalized to that of their corresponding mixed amino acid standard mass
538 chromatograms.
539
540

12

541

Fig. S2. The Hayabusa particles analyzed here were carbon-rich grains. Prior to amino acid analysis, the Hayabusa particles were analyzed by SEM-EDX, which revealed evidence of organic signatures, such as elemental C, N, and O. SEM-EDX analyses showed elemental compositions for particles #12 (A), #29 (B), #52 (C), #78 (D), and #80 (E), consistent with those described at the JAXA Hayabusa curation facility website (https://curation.isas.jaxa.jp/curation/hayabusa/, accessed 02 February 2022). The spectra shown here are the result of spot analyses. The particles displayed some heterogeneity, but the SEM spectra are representative of the C-rich areas of each grain.
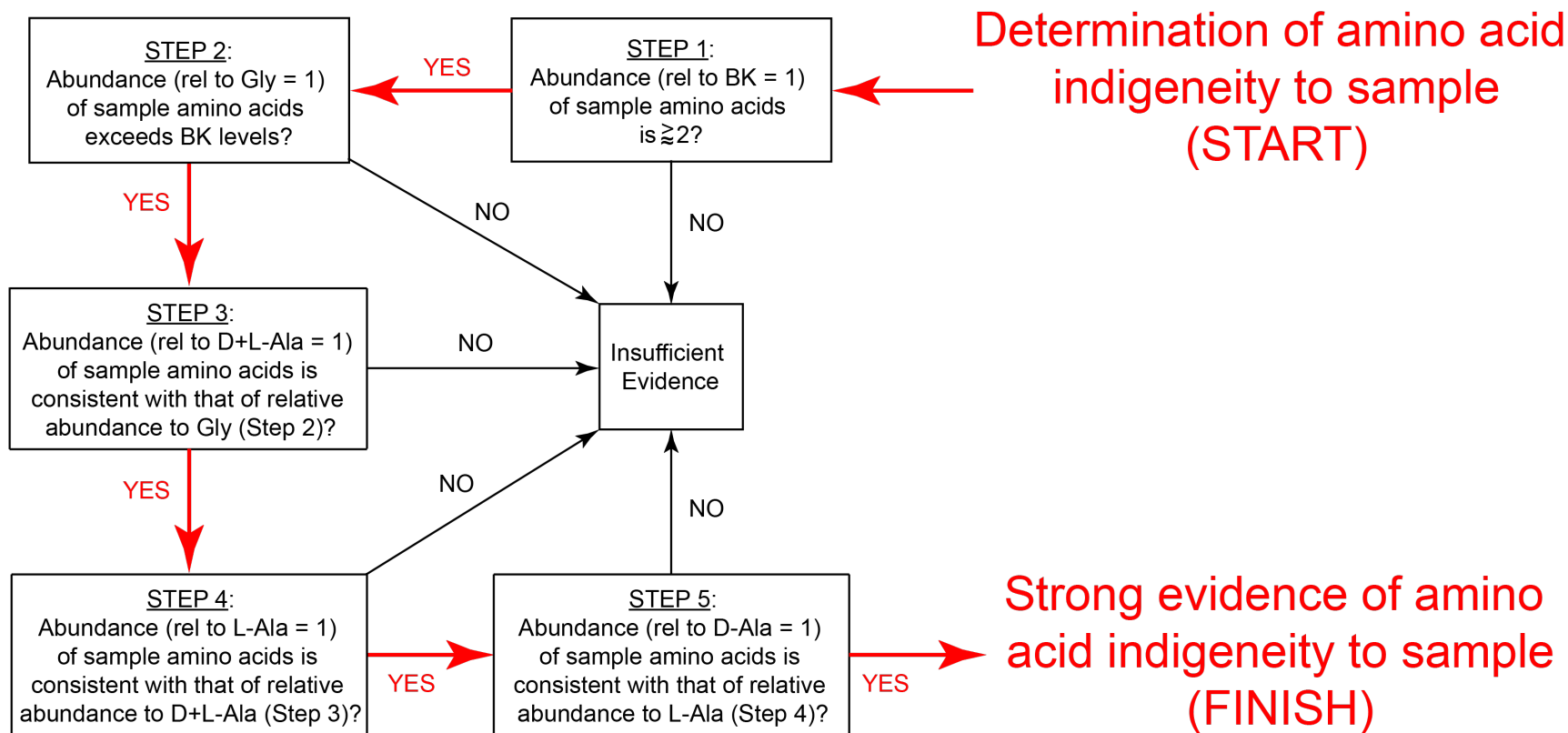
Fig. S3. Schematic of data analysis method employed to determine that strong evidence existed to suggest a portion of the abundance of a detected amino acid was indigenous to the sample. The highlighted route in red exhibits the path used to determine that quantitated sample amino acid abundances were likely to be at least partially indigenous to the sample, as opposed to being solely a product of contamination. If the evaluation criteria of fewer than all five steps of this data analysis method were satisfied by a given amino acid, it was determined that there was insufficient evidence to suggest the amino acid in question was at least partially indigenous to the sample.
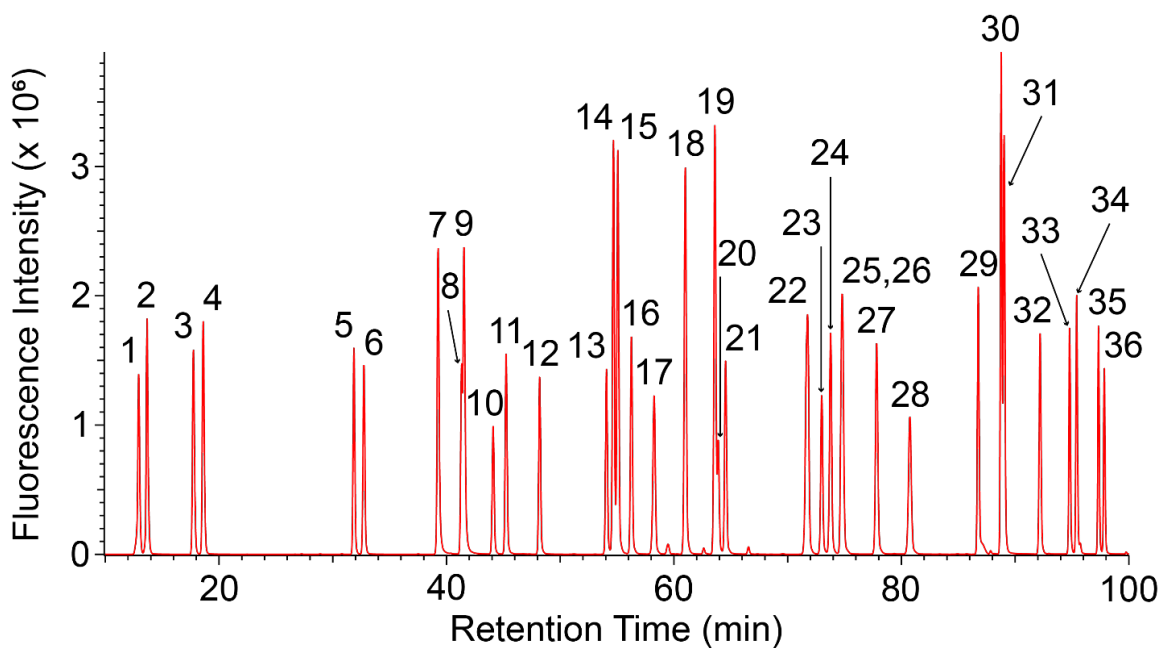
14

Fig. S4. A total of 36 analytes were analyzed for by the analytical technique employed here.
The 10 – 100-minute region of a fluorescence chromatogram of a mixed amino acid standard.
Select amino acids experienced some chromatographic coelution; however, all amino acids that
were not fully resolved by chromatography, alone, were fully resolved by a combination of
chromatography and accurate mass analysis, except for the enantiomers of α-ABA and Nva.
Analyte identifications shown here are consistent with those detailed in Table S2, and are as
follows: 1 = D-Asp, 2 = L-Asp, 3 = L-Glu, 4 = D-Glu, 5 = D-Ser, 6 = L-Ser, 7 = D-Ise, 8 = D-Thr, 9
= L-Ise, 10 = L-Thr, 11 = Gly, 12 = β-Ala, 13 = γ-ABA, 14 = D-β-AIB, 15 = L-β-AIB, 16 = D-Ala, 17
= L-Ala, 18 = D-β-ABA, 19 = L-β-ABA, 20 = δ-AVA, 21 = α-AIB, 22 = D,L-α-ABA, 23 = D-Iva, 24 =
S-3-APA, 25 = ε-ACA, 26 = L-Iva, 27 = R-3-APA, 28 = L-Val, 29 = D-Val, 30 = D-Nva, 31 = L-Nva,
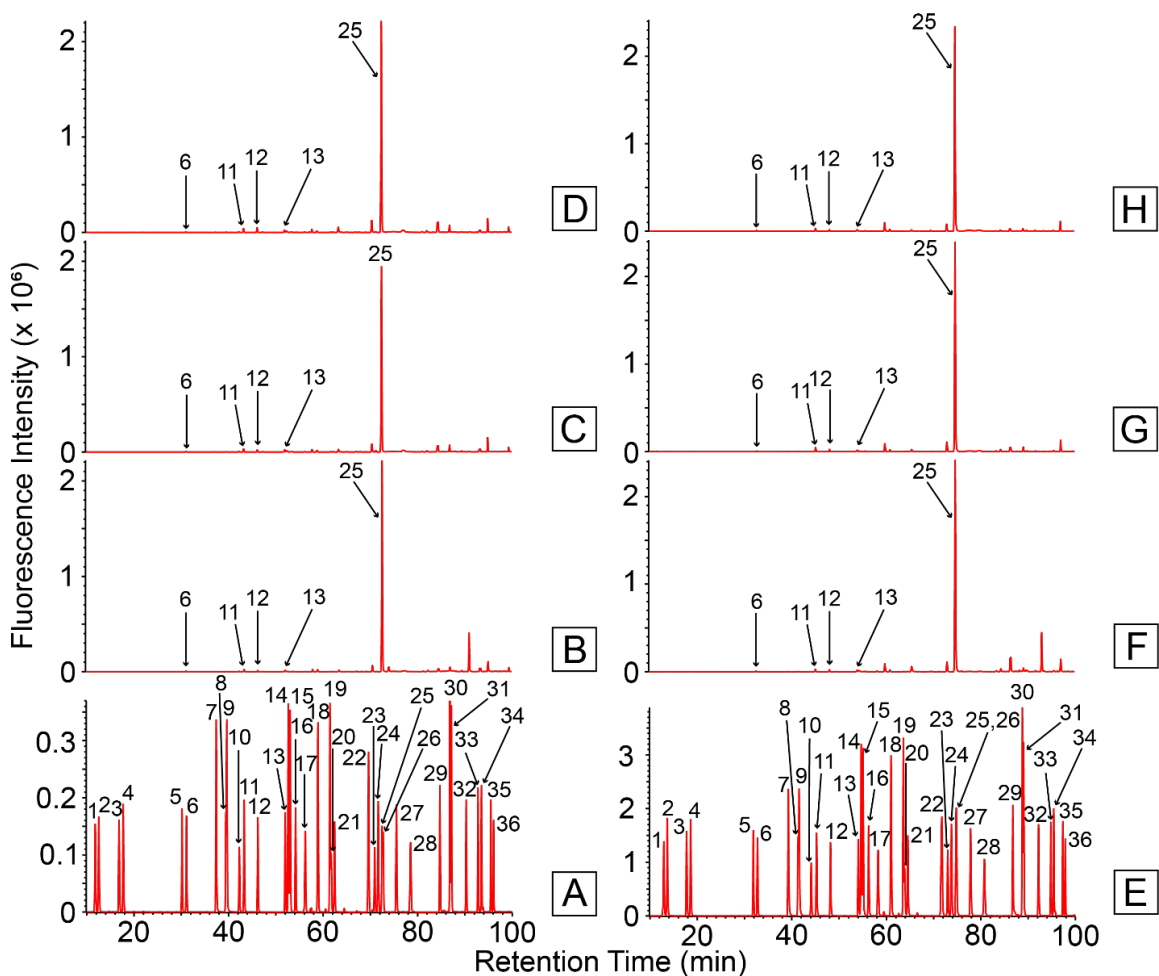32 = L-Ile, 33 = 8-AOA, 34 = D-Ile, 35 = D-Leu, 36 = L-Leu.

Fig. S5. The samples and procedural blank were found to be contaminated with ε-ACA; however, contamination did not prevent the detection of other amino acids. The 10 – 100-minute fluorescence chromatograms of a mixed amino acid standard (A and E), a blank (B and F), Murchison and #52 (C and G, respectively), and #12,29,80 and #78 (D and H, respectively). The most prominent analyte observed in the blank and samples was the background contaminant, ε-ACA (peak 25). However, the presence of this background contaminant did not prevent the detection of other species that were present at relatively small abundances, such as glycine, β-Ala, and γ-ABA. Analyte identifications shown here are consistent with those detailed in Table S2.
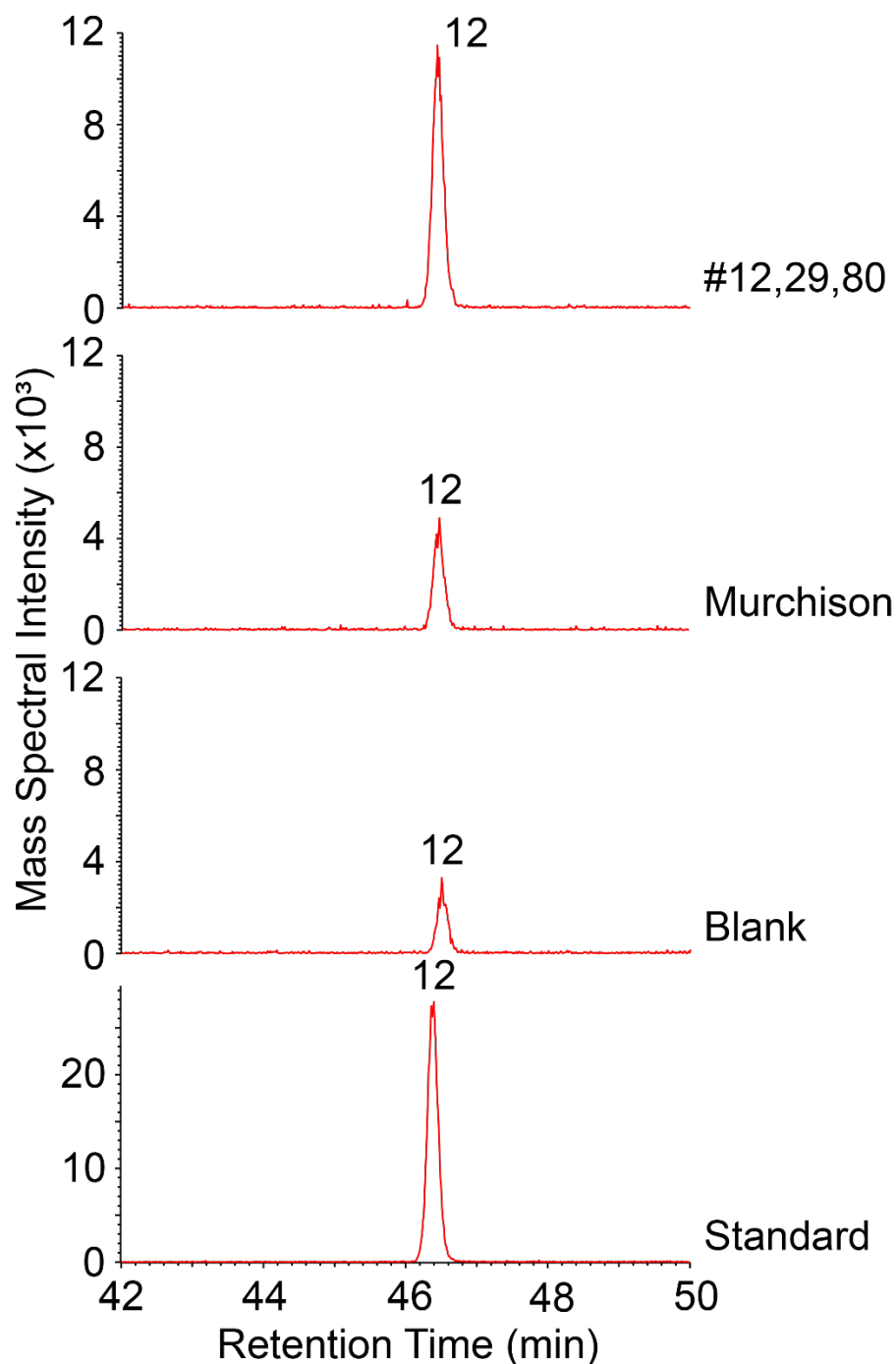
Fig. S6. Accurate mass chromatograms indicate detection of *β*-Ala in Murchison and #12,29,80. Analysis of β-Ala in a mixed amino acid standard, the procedural blank, Murchison, and #12,29,80, as depicted by their respective 42 - 50-minute accurate mass chromatograms for the *m/z* 351.1015 ± 10 ppm trace. Analyte identifications are consistent with those detailed in Table S2. The β-Ala peak in #12,29,80 is significantly larger than that in the procedural blank, suggesting that while some of the β-Ala signal detected in #12,29,80 is contributed by the blank, a large portion of the β-Ala signal in #12,29,80 may be indigenous to the sample.
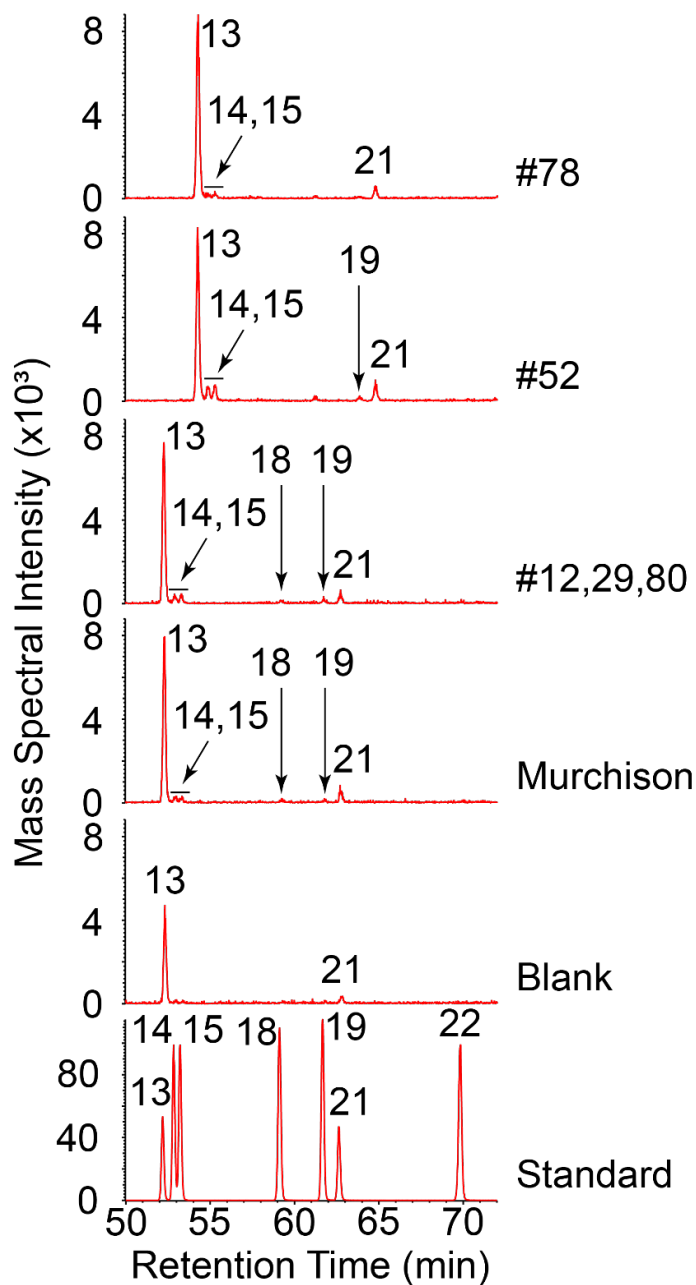
17

Fig. S7. Accurate mass chromatograms indicate detection of β-AIB and β-ABA in samples analyzed here. Analyses of C4 non-protein amino acids in a mixed amino acid standard, the procedural blank, Murchison, #12,29,80, #52, and #78, as depicted by their respective 50 – 72-minute accurate mass chromatograms for the *m/z* 365.1171 ± 10 ppm trace. Analyte identifications are consistent with those detailed in Table S2 and are as follows: 13 = γ-ABA, 14 = D-β-AIB, 15 = L-β-AIB, 18 = D-β-ABA, 19 = L-β-ABA, 21 = α-AIB, 22 = D,L-α-ABA. Small quantities of β-AIB were detected in all samples and low abundances of β-ABA were detected primarily in Murchison and #12,29,80. Note: retention times of analytes were shifted for #78 and #52 because these two samples were analyzed on a different day than were the Murchison and #12,29,80 samples.
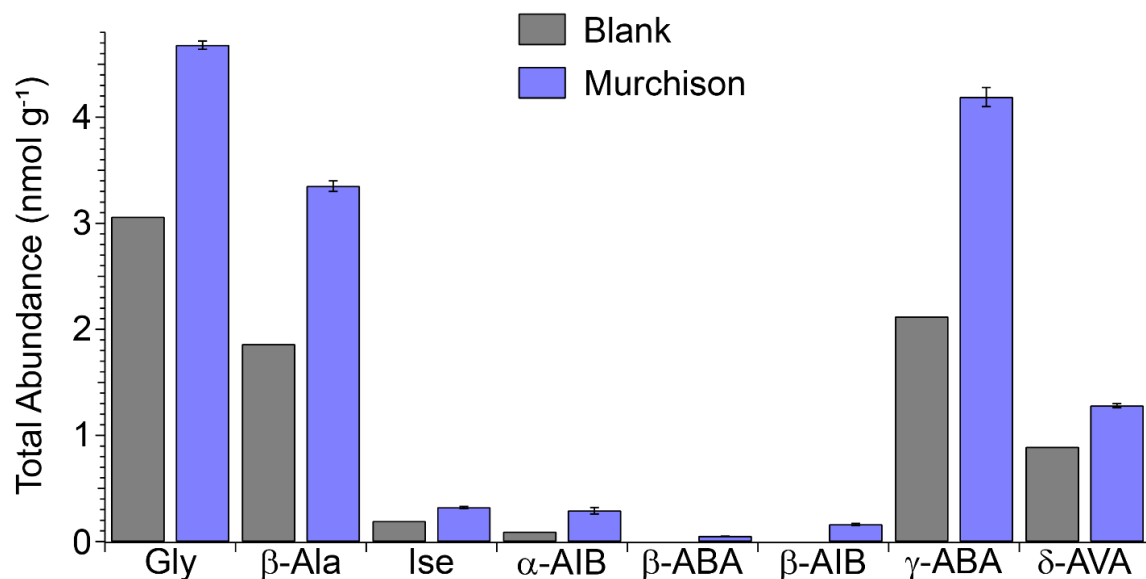
18

Fig. S8. Several species were detected above blank levels in the Murchison sample. Blank-uncorrected total abundances of select C_3 to C_5 non-protein amino acids and glycine observed in Murchison compared to corresponding blank levels. Several non-protein amino acids and glycine were observed in Murchison at abundances greater than blank levels. The standard errors reported here were taken from Table 2 of the Main Manuscript. Note: uncertainties of blank abundances are not shown because replicate blank measurements were not made. However, replicate measurements of other laboratory blanks have indicated that background amino acid abundances have similar uncertainties to those reported in the sample extracts.

Fig. S9. Particle #52 was depleted in amino acids relative to blank levels. Blank-uncorrected total abundances of select C_3 to C_5 non-protein amino acids and glycine observed in #52 compared to corresponding blank levels. The non-protein amino acids, β-ABA and β-AIB were detected at low abundances compared to blank levels, while the other amino acids were depleted relative to blank levels. The standard errors reported here were taken from Table 2 of the Main Manuscript. Uncertainties of blank relative abundances are not available because of reasons stated in the Fig. S8 legend.
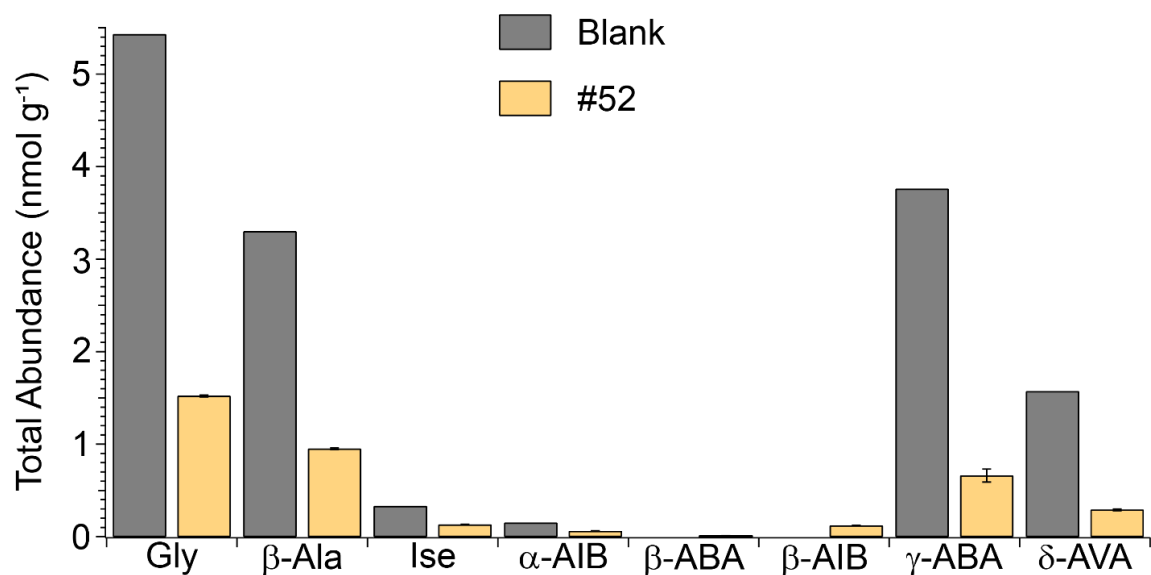
Fig. S10. Particle #78, like #52, was depleted in amino acids relative to blank levels. Blank-uncorrected total abundances of select C_3 to C_5 non-protein amino acids and glycine observed in #78 compared to corresponding blank levels. The non-protein amino acid, β-AIB was detected at low abundances, but the other species depicted here did not exceed blank levels. The standard errors reported here were taken from Table 2 of the Main Manuscript. Uncertainties of blank relative abundances are not available because of reasons stated in the Fig. S8 legend.
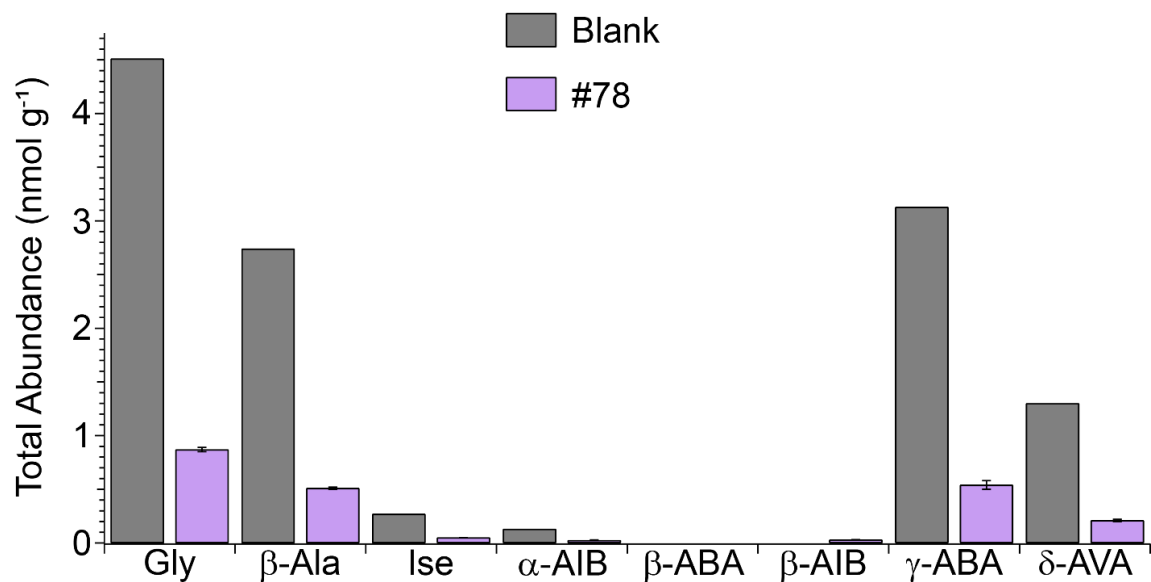
Fig. S11. Comparisons of amino acid abundances in samples relative to blank levels indicate that select species in Murchison and #12,29,80 are present at abundances distinct from blank levels and thus may be native to their respective samples. Blank-uncorrected abundances, relative to their corresponding blank levels, of select C_3 to C_5 non-protein amino acids and glycine observed in the samples analyzed here. The sample species whose abundances are most strikingly different from blank levels are β-Ala, Ise, and γ-ABA in #12,29,80, and α-AIB and γ-ABA in Murchison. The non-protein amino acids, β-AIB and β-ABA are not included in this comparison because these species were below detection limits in the procedural blank. Note: uncertainty estimates are not provided for amino acid abundances relative to blank levels because of reasons stated in the Fig. S8 legend. Therefore, blank uncertainty estimates were not available to propagate through the appropriate equations.
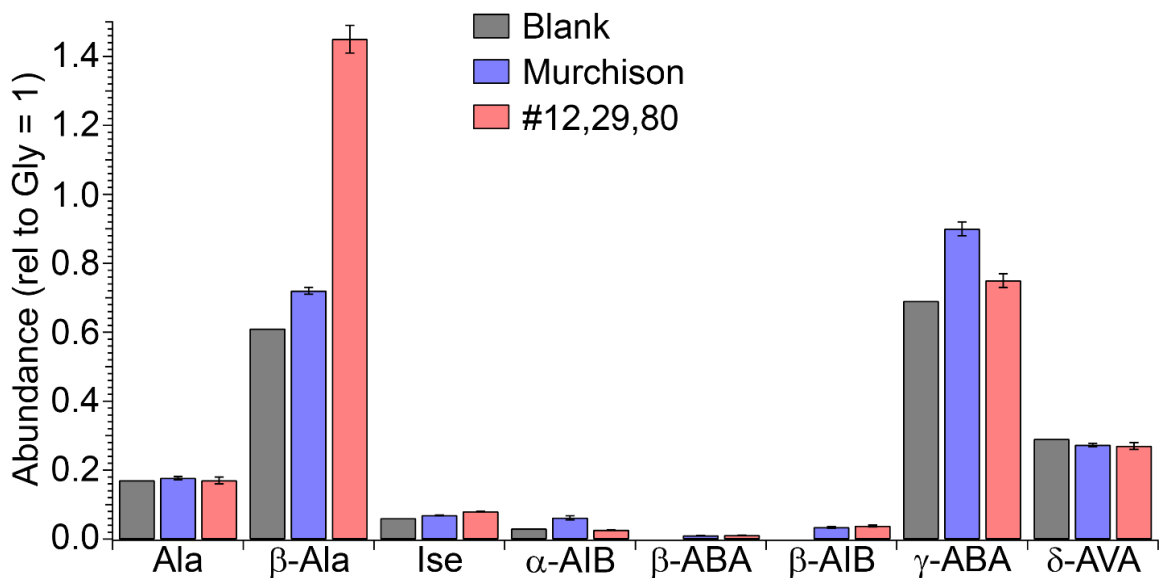
Fig. S12. The enlarged relative abundance of *β-Ala* in #12,29,80 supports the hypothesis that a portion of this non-protein amino acid's abundance is likely to be native to the grains analyzed. Blank-uncorrected abundances, relative to glycine, of select non-protein amino acids and alanine observed in the Murchison and #12,29,80 samples studied here. Sample relative abundances are compared to those of the procedural blank to distinguish which sample amino acid relative abundances exceed those of blank levels beyond sample measurement analytical errors, and are therefore likely to have been contributed by the sample. The standard errors reported here were based on the average values and associated standard errors reported in Table 2 of the Main Manuscript, and propagated through the appropriate equations. Uncertainties of blank relative abundances are not available because of reasons stated in the Fig. S8 legend.
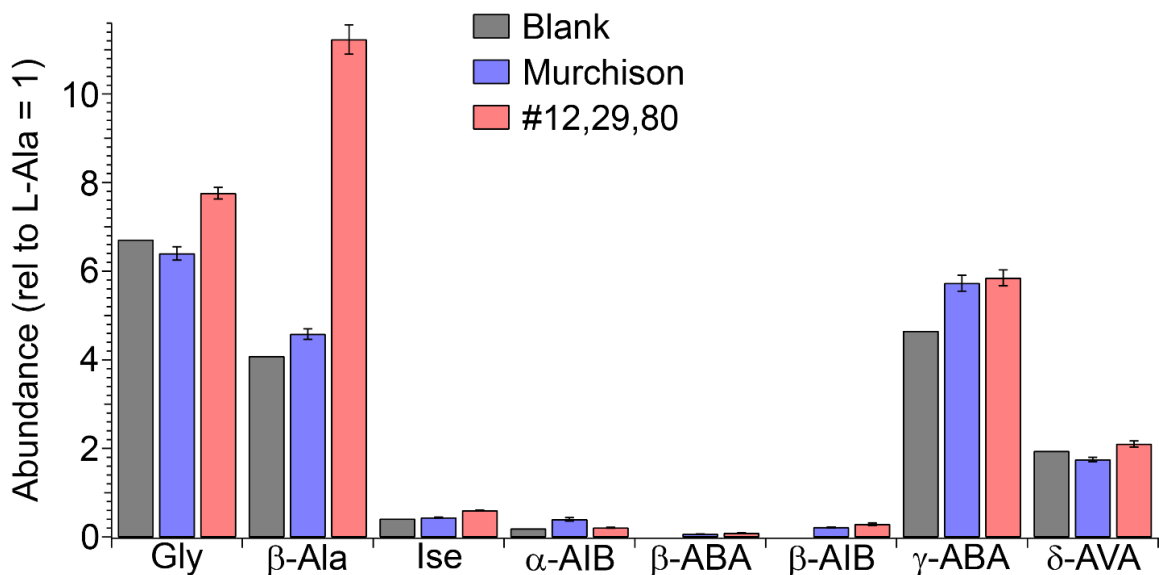
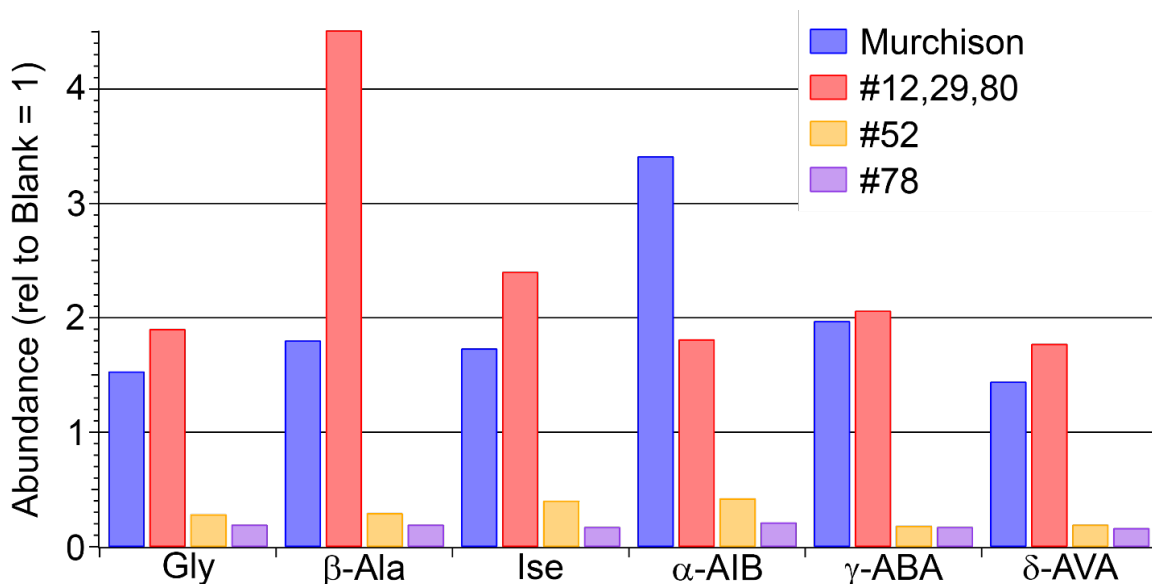**Fig. S13. The pronounced relative abundance of *β-Ala* in #12,29,80 suggests this non-protein amino acid's abundance is easily distinguishable from blank levels and thus likely to be native to the sample.** Blank-uncorrected abundances, relative to L-Ala, of select non-protein amino acids and glycine observed in Murchison and #12,29,80. Sample relative abundances are compared to those of the procedural blank to assess the likelihood these sample amino acids may have been contributed by their respective grains. The standard errors reported here were based on the average values and associated standard errors reported in Table 2 of the Main Manuscript, and propagated through the appropriate equations. Uncertainties of blank relative abundances are not available because of reasons stated in the Fig. S8 legend.
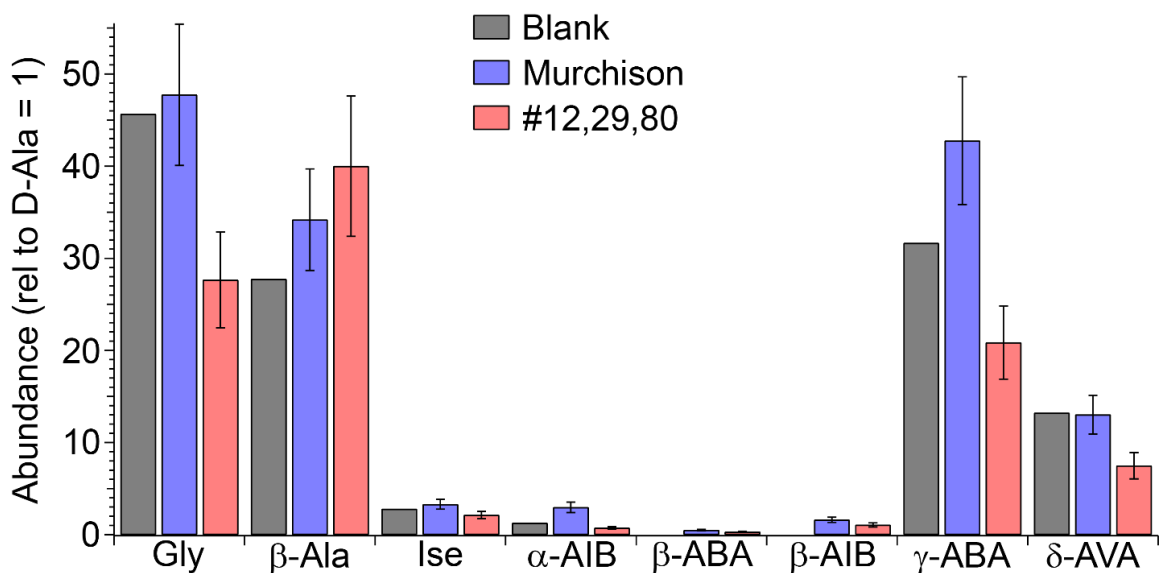
Fig. S14. The abundance, relative to D-Ala, of β-Ala for #12,29,80 remains consistently large, but that of γ-ABA drops in contrast to previous relative abundance profiles observed for γ-ABA. Blank-uncorrected abundances, relative to D-Ala, of select non-protein amino acids and glycine observed in Murchison and #12,29,80, compared to blank levels. While the relative abundance profiles of β-Ala for #12,29,80, α-AIB for Murchison, and β-ABA and β-AIB for both Murchison and #12,29,80 remain consistent with previous relative abundance profiles (Fig. S12, S13) and thus suggest they are indigenous to their respective samples, it is noteworthy that the relative abundance profile of γ-ABA for #12,29,80 is strikingly distinct from the previously observed relative abundance profiles of γ-ABA for #12,29,80 (Fig. S12, S13). This contrast indicates that the abundance of γ-ABA for #12,29,80 may likely be more heavily indigenous to the blank than the sample, itself. The standard errors reported here were based on the average values and associated standard errors reported in Table 2 of the Main Manuscript, and propagated through the appropriate equations. Uncertainties of blank relative abundances are not available because of reasons stated in the Fig. S8 legend.

Table S1. Post-hydrolysis reconstitution volumes and derivatization volumes of the gold foil procedural blank, the Hayabusa particles, and the Murchison sample extracted for amino acid analyses in this study.

Specimens	Post-hydrolysis reconstitution volume (μL)	Derivatization Volumes (μL)
Gold Foil Procedural Blank	125	110.102
Murchison	125	109.239
#12,29,80	125	105.973
#52	125	109.173
#78	125	107.966

Table S2. Detection metrics observed when analyzing a mixed amino acid standard using the analytical technique described in this study.

Analyte Number	Analyte	FD RT (min)	MS RT (min)	[M+H]$^+$ Chemical Formula	Theoretical m/z	Experimental m/z	Mass Error (ppm)
1	D-Asp	12.93	13.13	$C_{17}H_{19}N_2O_7S$	395.0913	395.0920	1.7717
2	L-Asp	13.67	13.87	$C_{17}H_{19}N_2O_7S$	395.0913	395.0919	1.5186
3	L-Glu	17.75	17.96	$C_{18}H_{21}N_2O_7S$	409.1069	409.1074	1.2222
4	D-Glu	18.60	18.81	$C_{18}H_{21}N_2O_7S$	409.1069	409.1079	2.4443
5	D-Ser	31.87	32.08	$C_{16}H_{19}N_2O_6S$	367.0964	367.0972	2.1793
6	L-Ser	32.73	32.97	$C_{16}H_{19}N_2O_6S$	367.0964	367.0972	2.1793
7	D-Ise	39.27	39.47	$C_{16}H_{19}N_2O_6S$	367.0964	367.0973	2.4517
8	D-Thr	41.33	41.53	$C_{17}H_{21}N_2O_6S$	381.1120	381.1133	3.4111
9	L-Ise	41.53	41.75	$C_{16}H_{19}N_2O_6S$	367.0964	367.0974	2.7241
10	L-Thr	44.10	44.31	$C_{17}H_{21}N_2O_6S$	381.1120	381.1140	5.2478
11	Gly	45.25	45.46	$C_{15}H_{17}N_2O_5S$	337.0858	337.0870	3.5599
12	β-Ala	48.20	48.40	$C_{16}H_{19}N_2O_5S$	351.1015	351.1027	3.4178
13	γ-ABA	54.07	54.29	$C_{17}H_{21}N_2O_5S$	365.1171	365.1182	3.0127
14	D-β-AIB	54.68	54.89	$C_{17}H_{21}N_2O_5S$	365.1171	365.1183	3.2866
15	L-β-AIB	55.07	55.29	$C_{17}H_{21}N_2O_5S$	365.1171	365.1181	2.7388
16	D-Ala	56.25	56.48	$C_{16}H_{19}N_2O_5S$	351.1015	351.1027	3.4178
17	L-Ala	58.27	58.47	$C_{16}H_{19}N_2O_5S$	351.1015	351.1019	1.1393
18	D-β-ABA	61.00	61.22	$C_{17}H_{21}N_2O_5S$	365.1171	365.1161	-2.7388
19	L-β-ABA	63.60	63.80	$C_{17}H_{21}N_2O_5S$	365.1171	365.1186	4.1083
20	δ-AVA	63.90	64.12	$C_{18}H_{23}N_2O_5S$	379.1328	379.1340	3.1651
21	α-AIB	64.55	64.76	$C_{17}H_{21}N_2O_5S$	365.1171	365.1188	4.6560
22	D,L-α-ABA	71.75	71.94	$C_{17}H_{21}N_2O_5S$	365.1171	365.1183	3.2866
23	D-Iva	73.00	73.23	$C_{18}H_{23}N_2O_5S$	379.1328	379.1338	2.6376
24	S-3-APA	73.78	74.01	$C_{18}H_{23}N_2O_5S$	379.1328	379.1337	2.3738
25	ε-ACA	74.80	74.94	$C_{19}H_{25}N_2O_5S$	393.1484	393.1496	3.0523
26	L-Iva	74.80	75.10	$C_{18}H_{23}N_2O_5S$	379.1328	379.1339	2.9014
27	R-3-APA	77.82	78.06	$C_{18}H_{23}N_2O_5S$	379.1328	379.1339	2.9014
28	L-Val	80.75	80.98	$C_{18}H_{23}N_2O_5S$	379.1328	379.1339	2.9014
29	D-Val	86.75	86.99	$C_{18}H_{23}N_2O_5S$	379.1328	379.1345	4.4839
30	D-Nva	88.77	89.01	$C_{18}H_{23}N_2O_5S$	379.1328	379.1342	3.6926
31	L-Nva	89.03	89.27	$C_{18}H_{23}N_2O_5S$	379.1328	379.1343	3.9564
32	L-Ile	92.20	92.44	$C_{19}H_{25}N_2O_5S$	393.1484	393.1495	2.7979
33	8-AOA	94.80	95.02	$C_{21}H_{29}N_2O_5S$	421.1797	421.1804	1.6620
34	D-Ile	95.42	95.65	$C_{19}H_{25}N_2O_5S$	393.1484	393.1494	2.5436
35	D-Leu	97.33	97.58	$C_{19}H_{25}N_2O_5S$	393.1484	393.1493	2.2892
36	L-Leu	97.83	98.08	$C_{19}H_{25}N_2O_5S$	393.1484	393.1492	2.0349

Upon derivatization with OPA/NAC, amino acid masses were shifted by 261 Da. Mass error was calculated using the following equation: $[(mass_{experimental} - mass_{theoretical})/mass_{theoretical}] \times 10^6$. Analyte numbers shown here correspond to the peak numbers denoted in fluorescence chromatograms and accurate mass chromatograms located throughout the Main Manuscript and Supporting Information.

Table S3. Detection metrics of select non-protein amino acids and glycine in the samples studied here. Mass errors were calculated as described for Table S2.

Analyte	STD MS RT (min)[a]	Theoretical *m/z*	Murchison			#12,29,80		
			Sample MS RT (min)	Experimental *m/z*	Mass Error (ppm)	Sample MS RT (min)	Experimental *m/z*	Mass Error (ppm)
D-Ise[b]	37.57	367.0964	37.61	367.1093	35.1406	37.61	367.1052	23.9719
L-Ise[b]	39.82	367.0964	39.87	367.1076	30.5097	39.87	367.1085	32.9614
Gly[b]	43.49	337.0858	43.53	337.0736	-36.1926	43.52	337.0748	-32.6326
β-Ala	46.39	351.1015	46.41	351.1007	-2.2785	46.37	351.1006	-2.5634
γ-ABA	52.19	365.1171	52.21	365.1165	-1.6433	52.18	365.1160	-3.0127
D-β-AIB	52.83	365.1171	52.85	365.1146	-6.8471	52.85	365.1145	-7.1210
L-β-AIB	53.22	365.1171	53.28	365.1159	-3.2866	53.23	365.1158	-3.5605
D-β-ABA	59.11	365.1171	59.16	365.1159	-3.2866	59.12	365.1161	-2.7388
L-β-ABA	61.65	365.1171	61.71	365.1141	-8.2165	61.71	365.1186	4.1083
δ-AVA[b]	61.95	379.1328	62.01	379.1265	-16.6169	61.94	379.1284	-11.6054
α-AIB	62.62	365.1171	62.71	365.1176	1.3694	62.64	365.1186	4.1083

Analyte	STD MS RT (min)[a]	Theoretical *m/z*	#52			#78		
			Sample MS RT (min)	Experimental *m/z*	Mass Error (ppm)	Sample MS RT (min)	Experimental *m/z*	Mass Error (ppm)
D-Ise	39.47	367.0964	n.d.	n.d.	n.d.	n.d.	n.d.	n.d.
L-Ise	41.75	367.0964	n.d.	n.d.	n.d.	n.d.	n.d.	n.d.
Gly	45.46	337.0858	n.d.	n.d.	n.d.	n.d.	n.d.	n.d.
β-Ala	48.40	351.1015	n.d.	n.d.	n.d.	n.d.	n.d.	n.d.
γ-ABA	54.29	365.1171	n.d.	n.d.	n.d.	n.d.	n.d.	n.d.
D-β-AIB	54.89	365.1171	54.90	365.1176	1.3694	54.90	365.1178	1.9172
L-β-AIB	55.29	365.1171	55.26	365.1173	0.5478	55.27	365.1173	0.5478
D-β-ABA[c]	61.22	365.1171	61.23	365.1078	-25.4713	n.d.	n.d.	n.d.
L-β-ABA	63.80	365.1171	63.83	365.1176	1.3694	n.d.	n.d.	n.d.
δ-AVA	64.12	379.1328	n.d.	n.d.	n.d.	n.d.	n.d.	n.d.
α-AIB	64.76	365.1171	n.d.	n.d.	n.d.	n.d.	n.d.	n.d.

n.d. = not determined because analyte abundance did not exceed blank levels.

[a] STD MS RT values differ slightly between the upper and lower portions of the table because the standards and corresponding samples in the upper portion of the table were run on a different day than those of the lower portion of the table.

[b] Target analyte was tentatively detected by retention time and optical fluorescence, compared to an analytical standard. However, unambiguous identification of the target analyte was not confirmed because the experimental mass of the target analyte exceeded the 10-ppm mass tolerance due to an unidentified, interfering analyte that possessed a nearly identical combination of retention time and experimental mass as the target analyte. Consequently, abundances reported in Table 2 of the Main Manuscript are based on optical fluorescence and serve as upper limit estimates.

[c] Unambiguous identification of the target analyte was not confirmed for #52 because an unidentified analyte that coeluted with the target analyte via optical fluorescence and also possessed an experimental accurate mass that overlapped with that of the target analyte, caused the measured experimental accurate mass of the target analyte in #52 to exceed the 10-ppm mass tolerance used. Consequently, quantitation was not performed.

Table S4. Summary of the D/L ratios and L_{ee} measured for select amino acids in the acid hydrolyzed hot water extracts of the CM2 Murchison grain and Hayabusa particles analyzed here.

C #	Amine Position	Amino Acid	Murchison (Glavin et al., 2021), (0.08 g)		Murchison (present work), (3.82 μg)		#12,29,80 (0.20 μg)		#52 (0.13 μg)		#78 (0.34 μg)	
			D/L Ratio	% L_{ee}	D/L Ratio	% L_{ee}	D/L Ratio	% L_{ee}	D/L Ratio	% L_{ee}	D/L Ratio	% L_{ee}
3	α	Ala	0.7 ± 0.1	15.4 ± 3.5	0.11 ± 0.06	79.8 ± 6.6	0.5 ± 0.1	34.3 ± 9.7	n.d.	n.d.	n.d.	n.d.
3	β	Ise	N.R.	N.R.	0.64 ± 0.05	22.0 ± 3.4	0.69 ± 0.03	18.2 ± 1.7	n.d.	n.d.	n.d.	n.d.
4	B	β-ABA	1.13 ± 0.09	-5.9 ± 4.4	0.96 ± 0.04[a]	1.9 ± 2.0[a]	0.9 ± 0.1[a]	3.04 ± 5.65[a]	§	§	n.d.	n.d.
4	B	β-AIB	⊥	⊥	1.2 ± 0.1[a]	-7.5 ± 7.0[a]	1.1 ± 0.2[a]	-6.8 ± 9.2[a]	1.03 ± 0.04[a]	-1.5 ± 1.7[a]	1.19 ± 0.09[a]	-8.7 ± 4.2[a]

For comparison purposes, data of the identical analytes measured in the acid hydrolyzed (total) hot water extract of a 0.08 g Murchison specimen (Glavin et al., 2021) are provided here. All data reported in the table from the current study are based on quantitation via optical fluorescence, except where noted below. The standard errors for the D/L ratios and L_{ee} reported here are based on the average values and associated standard errors reported in Table 2 of the Main Manuscript and propagated through the appropriate equations whereby $\%L_{ee} = [(1 - D/L)/(1 + D/L)] \times 100$.

n.d. = Not determined because analyte did not exceed blank levels.

N.R. = Values not reported.

⊥ Values not provided because the enantiomers were not separated by the chromatographic gradient used.

§ = Enantiomeric data not provided because unambiguous identification of the target analyte was not confirmed due to an optically fluorescent, coeluting, unidentified analyte that possessed an interfering experimental mass with the target analyte, causing the experimental mass of the target analyte to exceed the 10-ppm mass tolerance used. Consequently, quantitation was not performed.

[a] Quantitation of analytes measured in current study was performed via ToF-MS due to the presence of interfering species observed by optical fluorescence that were not observed when performing accurate mass analyses.

LEGENDS FOR DATASETS

Dataset S1. This dataset provides the raw data used to generate the fluorescence chromatograms of Fig. 2 of the Main Manuscript, which shows the 11- to 63-minute regions of the fluorescence chromatograms for a mixed amino acid standard, the procedural blank, Murchison, and #12,29,80.

Dataset S2. This dataset provides raw data to generate the mass chromatograms shown in Fig. S1 of the Supporting Information, which illustrates background amino acid abundances present in the analytical reagents used during sample preparation and analysis. In particular, the ultrapure water used for hot water extraction, the tdHCl used for acid vapor hydrolysis, and the derivatization materials were all evaluated for cleanliness prior to exposing samples to these reagents. This test provided a baseline appraisal of amino acid abundance uncertainties contributed by sample preparation and derivatization. This test revealed only small amounts of Gly and L-Ala were detected in select reagents used, indicating it is unlikely that large uncertainties in the observed amino acid abundances, namely β-Ala, were introduced by the wet chemical procedures (*i.e.,* extraction, hydrolysis, and derivatization) used here.

Dataset S3. This dataset provides the raw data used to generate the SEM-EDX spectra shown in Fig. S2 of the Supporting Information. Fig. S2 of the Supporting Information shows that the Hayabusa particles analyzed here were carbon-rich and contained such organic signatures as elemental C, N, and O.

Dataset S4. This dataset provides the raw data used to generate the fluorescence chromatograms shown in Fig. S4 of the Supporting Information. Fig. S4 of the Supporting Information shows the 10 – 100-minute region of a fluorescence chromatogram of a mixed amino acid standard. Select amino acids experienced some chromatographic coelution; however, all amino acids that were not fully resolved by chromatography, alone, were fully resolved by a combination of chromatography and accurate mass analysis, except for the enantiomers of α-ABA and Nva.

Dataset S5. This dataset provides the raw data used to generate the fluorescence chromatograms of Fig. S5 of the Supporting Information, which show the 10 – 100-minute chromatograms of a mixed amino acid standard (A and E), a blank (B and F), Murchison and #52 (C and G, respectively), and #12,29,80 and #78 (D and H, respectively). The most prominent analyte observed was the background contaminant, ε-ACA (peak 25). However, the presence of this background contaminant did not prevent the detection of other species present at small abundances (*e.g.,* Gly, β-Ala, and γ-ABA).

Dataset S6. This dataset provides the raw data used to generate the accurate mass chromatograms shown in Fig. S6 of the Supporting Information. Fig. S6 of the Supporting Information shows data from the analysis of β-Ala in a mixed amino acid standard, the procedural blank, Murchison, and #12,29,80, as depicted by their respective 42 - 50-minute accurate mass chromatograms for the *m/z* 351.1015 ± 10 ppm trace. The β-Ala peak in #12,29,80 is significantly larger than that in the procedural blank, suggesting that while some of the β-Ala signal detected in #12,29,80 is contributed by the blank, a large portion of the β-Ala signal in #12,29,80 may be indigenous to the sample.

Dataset S7. This dataset provides the raw data used to generate the accurate mass chromatograms shown in Fig. S7 of the Supporting Information. Fig. S7 of the Supporting Information shows data from the analysis of C_4 non-protein amino acids in a mixed amino acid standard, the procedural blank, Murchison, #12,29,80, #52, and #78, as depicted by their respective 50 – 72-minute accurate mass chromatograms for the *m/z* 365.1171 ± 10 ppm trace. Small quantities of β-AIB were detected in all samples, and low abundances of β-ABA were detected primarily in Murchison and #12,29,80. Note: retention times of analytes were shifted for #78 and #52 because these two samples were analyzed on a different day than were the Murchison and #12,29,80 samples.